Physica Scripta. Vol. 45, 112–132, 1992.

Physics Basis for Compact Ignition Experiments

B. Coppi, M. Nassi and L. E. Sugiyama

Massachusetts Institute of Technology, Cambridge, MA 02139, U.S.A.

Received September 12, 1991; accepted November 28, 1991

Abstract

Compact ignition experiments can be designed to attain peak densities $n_0 \simeq 10^{21}\,m^{-3}$ reliably and to achieve "low temperature" D–T ignition under conditions where the heating power of the α-particles does not exceed twice the ohmic heating power. An average current density near $1\,kA/cm^2$ with a maximum plasma current $I_p \simeq 12\,MA$ are the reference design parameters of the representative Ignitor Ult machine. The peak density value is consistent with that of B/R_0, as $R_0 \simeq 1.3\,m$ and $B_T \simeq 13\,T$, when compared to the Alcator, FT, and TFTR machines. The vacuum toroidal field B_T is reinforced by the contribution of a large paramagnetic poloidal current ($I_p < 10\,MA$). The high values of the poloidal field $B_p (\simeq 3.9\,T)$ produce a strong rate of ohmic heating, while the corresponding high values of I_p ensure that most of the fusion α-particles can be confined to deposit their energy in the central part of the plasma column. The confinement parameter $n_o \tau_E$ is expected to exceed $\simeq 4 \times 10^{20}\,sec/m^3$ by a considerable margin on the basis of the confinement properties of plasmas with prevalent ohmic heating. The necessary degree of plasma purity ($Z_{eff} \lesssim 1.6$) is expected to be ensured by the high particle densities, the high magnetic fields and the relatively low values of the thermal loading on the first wall. Since ignition is achieved through transient conditions rather than, as is frequently assumed, a sequence of steady state conditions, numerical simulations have shown that the ohmic power can remain considerable up to ignition, when programming the rise of the plasma current and the particle density while gradually increasing the cross section of the plasma. The volume where the magnetic parameter $q \leqslant 1$ and macroscopic $m^0 = 1$ plasma modes may be excited, has been shown to maintain quite low values until ignition is attained. The stability margin against these modes is made uniquely favorable by the low values of β-poloidal that are characteristic of Ignitor. An injected heating source of 16 MW of ICRF power is included to broaden the scenarios under which ignition is achieved.

List of symbols used in the tables

t	time
t_{ign}	ignition time
R_o	major radius of the plasma column
a	minor radius of the plasma cross section
κ	elongation of the plasma cross section
δ_G	triangularity of the plasma cross section
S_0	plasma surface
l_i	internal inductance
β_p	poloidal beta
β	toroidal beta
β_α	α-particle toroidal beta
n_{eo}	peak electron density
$\langle n_e \rangle$	volume averaged electron density
$\dot{n}$	rate of change of the plasma density
$n_{\alpha o}$	peak thermal α-particle density
q_o	plasma current safety factor at the plasma center
q_ψ	plasma current safety factor at the plasma edge
$Vol_{q=1}$	volume inside the surface where $q = 1$ (% of the total plasma volume)
$T_{q=1}$	temperature at the $q = 1$ surface at the time when its volume becomes equal to 10% of the total plasma volume
I_p	toroidal plasma current
I_{BS}	bootstrap current
T_{eo}	peak electron temperature
$\langle T_e \rangle$	volume averaged electron temperature
W_{int}	internal energy
$\dot{W}_{int}$	rate of change of the internal energy
τ_E	energy confinement time
P_{OH}	ohmic power
P_α	α-power
P_{INJ}	injected power
P_B	bremsstrahlung radiation power
P_{IC}	cyclotron and carbon impurity radiation power
P_L	total power losses
V–s	linked magnetic flux variation
γ_i	numerical coefficient defining the ratio of ion and electron nonohmic thermal conductivities
Z_{eff}	effective charge

1. Introduction

Compact experiments have been the first [1] to be proposed in order to achieve fusion ignition conditions on the basis of existing technology and the available knowledge of the physics of well-confined plasmas. At ignition, in a deuterium–tritium plasma, the power released to the plasma by the 3.5 MeV α-particles produced by fusion reactions equals the total of all forms of energy loss from the plasma. The favorable confinement properties of high density plasmas, discovered by the series of experiments carried out by the high field Alcator machines at MIT, have made it possible to conceive of experiments capable of attaining ignition at low temperature, under the most conservative (i.e., least extrapolated) conditions relative to the physical regimes that have been attained so far in magnetically confined plasmas. By low temperature ignition, we mean that the peak plasma temperature T_o is less than or about 15 keV, requiring values of the confinement parameters $n_o \tau_E \gtrsim 4 \times 10^{20}\,sec/m^3$, where n_o is the peak density of the fusing nuclei and τ_E the plasma energy replacement time. The typical values that are considered for n_o are about $10^{21}\,m^{-3}$. These are compatible with the possibility to reach

ignition with peak temperature as low as 11 keV when the rate of ohmic heating remains strong relative to that of α-particle heating and the relevant confinement times are consistent with those of existing experiments in regimes where the rate of ohmic heating is significant.

An important feature of compact high magnetic field experiments is the strong rate of ohmic heating they can produce. Therefore, they have the potential to achieve fusion burning and ignition conditions without injected heating systems. Besides the evident costs and complexities associated with injected heating, the degradation of the energy confinement observed in connection with its application in present day experiments can be avoided. Thus the injected heating system (ICRH) that is included in the Ignitor design, with a maximum power of 16 MW, has the function of a backup. We observe that the values of the overall magnetic energies stored in compact ignition experiments are drastically lower than those of large volume experiments, with inferior expected performances, that are being studied at this time.

We note also that the first plasmas with a high degree of purity were obtained by the high particle density experiments performed with the Alcator machine and, since then, the observation that the degree of plasma purity increases with density has been widely confirmed.

The Ignitor experiment has been conceived from the beginning to take maximum advantage of the favorable characteristics of compact experiments for ignition, subject to the constraints imposed by currently available materials and technology. It will be used in the rest of the paper as the primary exemplar of the philosophy and the practical considerations underlying the achievement of ignition in a D–T plasma.

1.1. *Particle density and energy confinement*

The Ignitor experiment has been designed from the beginning to incorporate features that make attaining regimes where $n_o \tau_E \simeq 4 \times 10^{20}$ sec/m^3, at fusion burning conditions, possible with a considerable safety margin. In particular, peak particle densities n_o around 10^{21} m^{-3} should be obtainable, on the basis of the series of experiments started by the Alcator machines at MIT [2] and followed by the FT machine at Frascati and the TFTR at Princeton. Since the value of n_o obtained experimentally correlates with the ratio B/R_o, B being the magnetic field at the center of the plasma column, and R_o the torus major radius, the value of R_o in Ignitor (see Fig. 1 and Table I) has not been allowed to exceed twice that of the Alcator–C machine, where approximately twice the envisioned density, $n_o \simeq 2 \times 10^{21}$ m^{-3}, was achieved with comparable values of B, around 12.5 T. The maximum magnetic field in Ignitor is expected to approach this value with adequate reliability, considering also that the paramagnetic contribution of the plasma current is expected to add appreciably to the field produced by the toroidal magnet. In addition, we observe that the maximum value of $n_o R_o/B$ obtained by the TFTR experiments is well above that obtained by the Alcator–C machine. If the argument can be made that the maximum values of n_o may be related to the volume averaged toroidal current density $\langle J_\phi \rangle$, the reference maximum value for $\langle J_\phi \rangle$ to be achieved in Ignitor is $\simeq 0.93$ kA/cm^2, which is slightly higher than that attained by the Alcator–C experiments. Thus $n_o \simeq 10^{21}$ m^{-3} should be reached in Ignitor with a considerable degree of confidence.

Two other important features of the Ignitor design are the high values of the poloidal magnetic field B_p and the toroidal plasma current associated with it. The high values of B_p (up to 3.9 T) produce a strong rate of ohmic heating, while the corresponding high values of I_p (up to 12 MA) ensure that most of the α-particles produced by fusion reactions can be confined to deposit their energy in the central part of the plasma column. This is advantageous, as the diffusion coefficient for the plasma thermal energy is consistently found to be minimal in the central region. As indicated earlier, the Ignitor plasma configuration, featuring an elongated cross section and a tight aspect ratio, also ensures the presence of a (paramagnetic) plasma current I_θ, flowing in the poloidal direction in addition to the toroidal plasma current I_p. The component I_θ can approach 10 MA when the parameter $\beta_p = 8\pi\langle p \rangle / B_p^2$, where $\langle p \rangle$ is the mean plasma pressure, is small.

In fact, the high mean values of the poloidal field that are considered make it possible to attain ignition conditions at a relatively low value of β_p. This ensures a considerable margin for stability against the onset of macroscopic internal (ideal MHD) modes with dominant poloidal mode number $m^0 = 1$ [3], that can hamper the attainment of ignition [4]. Section 5 is devoted to this general subject.

Moreover, high values of I_p can limit the degradation of the energy confinement time τ_E in the so-called L-regime, that is observed in present day experiments when an injected form of heating is applied and prevails over ohmic heating. This is an important consideration, as the margin by which the desired value of τ_E can be obtained is generally more difficult to predict than the attainable peak density. Clearly, if the energy confinement time follows the trend indicated by experiments where only ohmic heating is present [5, 6], the margin to obtain $\tau_E \simeq 0.4$ sec is relatively large (a factor of 2 to 3). The key factor then is the rate at which degradation may take place when the α-particle heating prevails over ohmic heating. On the other hand, Ignitor has the unique favorable feature that it can reach ignition where P_α, the power provided by α-particle heating, compensates for all forms of energy loss, but does not exceed $2P_{OH}$, P_{OH} being the power associated with ohmic heating. Then we notice that:

(*i*) The degradation of plasma confinement in present day experiments has been observed so far when ohmic heating becomes much smaller than other forms of heating, all of which are injected at discrete points around the torus. On the other hand, α-heating is internal to the plasma column and distributed axisymmetrically, two features that it has in common with ohmic heating that has optimal confinement characteristics.

(*ii*) In order to maintain a good margin for τ_E, the best strategy is to maintain a strong rate of ohmic heating up to relatively high temperatures when α-particle heating also begins to be strong. This is accomplished by programming the rise of the plasma current and the particle density while gradually increasing the cross section of the plasma column [7, 8]. By the end of this relatively long ($\gtrsim 3$ sec) transient phase the applied electric field is strongly inhomogeneous, being low at the center of the plasma column, where the temperature can achieve relatively high values, and finite at

the edge of the plasma column (corresponding to loop voltages $V_\phi \gtrsim 1$ V). The ohmic power input can then remain considerable up to ignition.

(*iii*) Provision has been made in the machine design for the so-called H-regime, where the confinement time is not degraded relative to that expected for regimes where only ohmic heating is present, when other forms of heating prevail. These consist of:

(*a*) A choice of machine parameters that enables the plasma column to maintain its reference dimensions and characteristics while having its outer edge detached from the first wall by a distance more than sufficient for the onset of the H-regime, a procedure suggested and confirmed by a significant set of experiments [9].

(*b*) An optimized set of poloidal field coils, placed in proximity to the plasma column, that can generate plasma equilibrium configurations with x-points, of the same type as those produced by divertors. In order to implement this provision it is necessary, however, to avoid the presence of narrow regions of the first wall where the thermal loading is too high and to keep the plasma current well below its maximum design value.

We observe that the improvement of the energy confinement time τ_E in the H-regime, over the values found in the L-regime, is due largely to the increase of thermal energy density in the outer region of the plasma column, whose contribution to the rate of fusion reactions is not major. Therefore, rather than having the primary goal of reproducing the H-regime of confinement in Ignitor we have adopted that of reaching ignition with the minimum value of P_α/P_{OH}. Nevertheless the design of Ignitor is consistent with "pessimistic" ignition scenarios where the energy confinement time has values typical of those that can be extrapolated for experiments in the L-regime.

Finally we point out that the Ignitor parameters and, if necessary, the use of a pellet injector, allow the production and maintenance of a density profile with the following characteristics:

– High peak values (the advantages of this have been mentioned already);

– Centrally peaked profile shape. This feature avoids the excitation of the long wavelength η_i-modes [10] and their contribution to the ion thermal energy transport [11], and may also act to suppress sawtooth oscillations (see Section 5.1);

– Relatively high edge density and thus high probability of interactions between plasma particles and neutrals as well as impurities. This implies:

- A high ionization rate of neutrals and consequently a high level of recycling;
- The ability to screen the main plasma from impurities and thus the possibility to achieve a low Z_{eff};
- A strong radiative cooling at the edge due to the impurities in the Scrape Off Layer. This corresponds to more uniformly distributed energy transfer to the first wall.

A series of experiments carried out by the FT and the FTU machines in high density plasmas with limiter configurations have shown that a high fraction of the plasma thermal energy ($\geqslant 50\%$) is carried to the first wall by radiation. Therefore, the peak values of the thermal wall loading can be expected to be modest in Ignitor, especially when ignition at temperatures below 15 keV can be achieved.

1.2. *Plasma purity and divertors*

An important requirement in order to achieve ignition conditions is that the plasma have a relatively high degree of purity. In practice, the parameter Z_{eff} that is a measure of the average charge of the plasma nuclei should not be higher than about 1.6 ($Z_{eff} = \sum_j n_j Z_j^2/n_e$, n_e = electron density, j indicates the nuclear species). This rough purity criterion was, in fact, first pointed out by us. The most reliable and proven way to keep Z_{eff} below the indicated value, according to experiments performed so far, is to produce plasmas with very high densities, in the range for which Ignitor has been designed. A long series of experiments have confirmed the observation made first by the Alcator machine [2] in late 1974, that Z_{eff} is a monotonically decreasing function of the density. The high values of the magnetic field and the expected low values of the thermal loads on the first wall expected in Ignitor under low temperature ignition conditions are further favorable factors to obtain the desired low values of Z_{eff}.

We note that the use of a divertor to improve the thermal energy confinement was proposed first in Ref. [10], that included one of us, when the favorable confinement characteristics of high density plasmas were not known. Therefore, the use of a divertor in Ignitor has been carefully considered since the beginning of the program. Reflecting this, the poloidal field system of Ignitor has been designed with sufficient flexibility to produce divertor configurations with double x-points at high currents. However, at the maximum plasma current, the machine design has considered only limiter configurations without x-points for the following reasons:

(*i*) Regimes with a high degree of purity have been obtained in high density plasmas, where the effectiveness of divertors to obtain low values of Z_{eff} has not been demonstrated yet.

(*ii*) The design of the plasma chamber and of the toroidal magnet would become considerably more complex.

(*iii*) To retain the divertor configuration at the highest currents, the major radius would have to undergo a large increase and the attainable values of B/R_o would be considerably degraded. This would undermine the margin by which peak densities $n_o \simeq 10^{21}\,\mathrm{m}^{-3}$ can be predicted to be produced and well confined.

(*iv*) The increased dimensions and lower magnetic fields would lead to lower values of the poloidal field B_p, even assuming that the maximum plasma current can be held at 12 MA, and decrease the maximum temperature achievable by ohmic heating alone, as well as the maximum plasma pressure that can be confined without driving macroscopic (ideal MHD) internal modes unstable.

(*v*) With the demise of ohmic heating a large and reliable injected heating system becomes necessary, rather than having the role of a backup. The issue of degraded confinement then becomes important well before α-particle heating begins to be a key component of the overall energy balance.

(*vi*) Relatively narrow regions (the divertor plates) where the thermal wall heating reaches very high values are introduced with operation in the divertor mode.

These circumstances render the objective of ignition very difficult to attain, if a divertor is required at the highest plasma current values. In addition, the compact nature of

the experiment, with the limit on costs, time scales, etc., that this characteristic involves, is lost. The design history of the CIT (Compact Ignition Tokamak) machine, proposed originally by one of us at the Princeton Plasma Physics Laboratory in 1984, is a good illustration of these arguments. In fact CIT, no longer compact nor maintaining the objective of ignition [12], has been renamed BPX (Burning Plasma Experiment).

2. Design parameters and characteristics

As indicated earlier the Ignitor experiment was suggested by the results [2] of the Alcator program developed at MIT that revealed the superior confinement properties and the high degree of purity of high density plasmas in compact, high magnetic field configurations. In addition, Ignitor was conceived using the same high field magnet technology as Alcator, that involves cryogenically cooled normal conductors. The minimum starting temperature (about 30 K) in Ignitor is determined by helium gas cooling, while in Alcator liquid nitrogen cooling was adopted with the minimum starting temperature about 80 K. The lower temperature and lower current densities in the toroidal magnet allowed by the design of Ignitor [13], $<10\,\mathrm{kA/cm^2}$ compared to $\sim 22\,\mathrm{kA/cm^2}$, the maximum reference value considered for the Alcator–C machine, makes Ignitor suitable for considerably longer plasma current pulses that can exceed $10\tau_E$, τ_E being the expected plasma energy replacement time at ignition.

The Ignitor experiment, since it was proposed, has undergone a process of upgrading and machine optimization [14], reflecting the experimental and theoretical advances that have been made in the physics of multi-keV plasmas. The Ignitor–Ult machine [7] is the latest embodiment of this process. Its design parameters are indicated in Table I and the machine's key elements are shown in Fig. 1.

A feature maintained throughout the evolution of the design of Ignitor is that of toroidal coil plates, connected in series externally and supported by an appropriate steel structure so as to withstand both the vertical (axial) and the horizontal (radial) electrodynamic forces. In particular, the loads on the inner leg of the toroidal magnet are supported by bucking between the toroidal and poloidal coils (with an appropriate sliding surface at the interface between the toroidal magnet and the air core transformer), by wedging between the inner part of the toroidal coils, and by external structural elements. These consist of (see Fig. 1):

– A set of steel plates ("C-clamps") surrounding each of the 24 modules of copper plates that compose the toroidal magnet. The C-clamps are wedged on the outside to allow the unwedged part to rotate around an effective hinge under the effect of the bracing rings. Thus only a small fraction of the vertical separating force is unloaded onto the central leg of the toroidal magnet.

– Two bracing rings maintaining the plate assembly and transferring the vertical separating force produced by the toroidal magnet to the effective outer shell formed by the steel plates.

– A central massive post filling the bore of the air core transformer whose main functions are to absorb the centripetal force acting on the inner leg of the toroidal magnet and

Table I. *Reference design parameters of the Ignitor Ult machine*

$R_o \simeq 1.30\,\mathrm{m}$	Major radius of the plasma column
$a \times b \simeq 0.47 \times 0.87\,\mathrm{m^2}$	Minor radii of the plasma cross section
$\delta_G \simeq 0.4$	Triangularity of the plasma cross section
$I_p \lesssim 12\,\mathrm{MA}$	Plasma current in the toroidal direction
$I_\phi \lesssim 10\,\mathrm{MA}$	Plasma current in the poloidal direction
$B_T \lesssim 13\,\mathrm{T}$	Field produced by the toroidal magnet
$\Delta B_T \lesssim 1.5\,\mathrm{T}$	Paramagnetic (additional) field produced by I_ϕ
$\langle J_\phi \rangle \lesssim 0.93\,\mathrm{kA/cm^2}$	Average toroidal current density
$\bar{B}_p \lesssim 3.75\,\mathrm{T}$	Mean poloidal field
$I_p \bar{B}_p \lesssim 45\,\mathrm{MN/m}$	Confinement strength parameter
$q_\psi \lesssim 3.6$	Edge magnetic safety factor at maximum plasma current
$V_o \simeq 9.5\,\mathrm{m^3}$	Plasma volume
$S_o \simeq 36\,\mathrm{m^2}$	Plasma surface
$W_j \simeq 16\,\mathrm{MW}$	Injected heating power (ICRH at $f \simeq 130\,\mathrm{MHz}$)

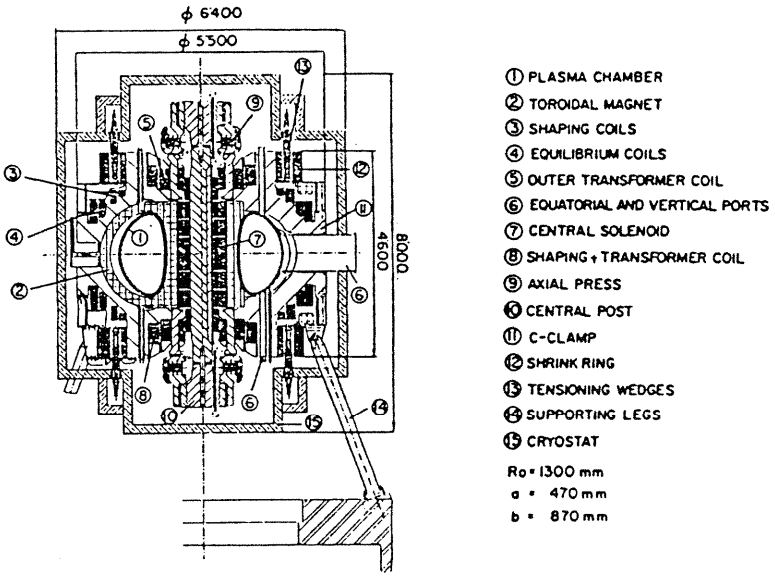

Fig. 1. Main components of the Ignitor machine

to be a component of a central press. Radial vertical cuts in the post are introduced to minimise the effects of the induced currents.

– A vertical electromagnetic press connected with the central post and capable of giving a compression preload on the inner leg of the toroidal magnet to reduce the electromagnetic load. The press is deactivated during the relevant current pulse as soon as the thermal expansion due to the temperature rise in the toroidal magnet becomes significant or whenever the machine is operated with magnetic fields below the maximum considered values.

The validity of the structural solution adopted for the Ignitor magnets has been verified by independent studies. In particular one of the latest considers its extension to a plasma configuration whose major radius is 2.1 m, which is called "Dignitor" [15], and shows the potential that this solution has for future experiments.

To avoid heating the magnets to temperatures which would endanger the mechanical integrity of the machine, a hybrid cryogenic system is adopted where the warmer part of the plant is operated with liquid N_2 and the colder part with He. Heat transfer from the coils to the coolant takes place through forced convection in conduits within the coils. The cooling time of the toroidal magnet down to a final temperature of about 30 K, after a pulse corresponding to the maximum plasma current scenario, is shorter than that for the central solenoid.

A highly optimized poloidal magnet system has the function of inducing the plasma current, creating the desired equilibrium configuration of the plasma column and maintaining it. The main component of this system is the central solenoid, the so-called air core transformer consisting of a double array of copper coils, wrapped 32 times around the central steel pole of the machine. Each conductor coil is provided with a cooling channel at its center. The cooling time of the central solenoid, down to about 30 K, after a current pulse corresponding to the maximum plasma current scenario, is of the order of hours.

An assessment of the magnetic flux variation linked with the plasma column, that has to be produced by the poloidal field system, is given in Ref. [16]. For plasma parameters resulting from the numerical simulations we have performed, the volt-second requirement to reach ignition ranges from 29 to 34 V-sec for ignition at the beginning or the end of the flat top phase of the discharge, respectively, with a 3 sec current ramp to the maximum value of the plasma current. The volt-second consumption during the flat top, at a rate of about 1.7 V-sec per second, is due to resistive losses as well as an inductive component corresponding to an increase in l_i. We note that in discharges aided by injected heating, where the plasma reaches ignition during the current ramp, at a lower plasma current, the requirement may be as low as $\simeq 25$ V-sec. Previous results showed that longer ramps (e.g. 4.5 sec) required only a small increase (e.g. $1 \div 2$ V/sec) in the volt-second requirement at ignition. These values can be delivered to the plasma by the poloidal field system as actually designed.

The adopted plasma chamber, made of Inconel 625, is divided into 24 sectors, joined by welding. The plasma chamber is mechanically supported and restrained by the C-clamps through the long ducts forming the horizontal ports, which allow freedom for deformation under electromagnetic and thermal loads. The plasma chamber acts as a support for the first wall system that is made of graphite tiles covering the entire inner surface. A set of tiles is attached to appropriate (double curvature) support plates that can be replaced by a remote handling system.

As shown in Fig. 1, vertical and equatorial access ports to the plasma chamber are provided for the diagnostic systems, the vacuum system, the pellet injector, the auxiliary heating, the remote handling system, etc. In particular, six of the twelve equatorial ports are designed to house the antennae of the r.f. heating system (ICRF). The estimated power that can be delivered from the antennae placed in each of the six housings is in the range 2.5 to 4.0 MW. Since Ignitor is designed to exploit fully the ohmic heating associated with the large currents induced in the plasma column, the main function of the injected heating system is to broaden the range of scenarios under which ignition can be obtained. In addition, ICRH can be used as a means to control the penetration of the current density, by locally heating specific regions of the plasma column, and to suppress the onset of $m^\circ = 1$ modes by the fast particle population it can produce within the $q = 1$ surface.

An injector of deuterium pellets (~ 4 mm diameter) is an important component of the Ignitor experiment. We note that relatively high pellet speeds are required to reach the center of the plasma column. The considered values are 2 km/sec or higher and have been achieved by existing technologies. The possible functions of a pellet injection system, to be used in addition to the well tested technique of gas injection ("puffing") [2], have been indicated in Section 2. Another use for a pellet injector that has been demonstrated recently is to condition the first wall by launching lithium pellets into the plasma column prior to regular hydrogenic discharges [17].

3. Approach to ignition conditions and transport

3.1. *General considerations for time evolution*

Many of the basic requirements for ignition depend upon the interaction of multiple temporally and spatially varying processes [18]. These include the development of the highest possible rate of ohmic heating within the plasma column, the avoidance of large scale and frequent sawtooth oscillations, the control of macroscopic instabilities in general, and the minimization of the thermal and particle transport. The current rise phase of the plasma, lasting several seconds in the case of Ignitor, plays an important part [7, 8] in these processes, as it forms the radial profiles of the plasma current and temperature, while also allowing means for their control. Ignition is most effectively achieved soon after the end of the current rise, to take advantage of the favorable conditions attained by this phase of the discharge in terms of broad toroidal current density profiles and thus small regions where $q < 1$. The effects of the current rise, however, persist for some time after the end of the ramp.

To study these effects, extensive numerical simulations of the current rise and subsequent phases of the discharge have been carried out with both free and fixed boundary transport codes. The free boundary simulations, using the TSC [19] code, are reported here. It solves the MHD and the flux surface transport equations in the region inside the pol-

oidal field coils to self-consistently model the plasma, the vacuum region, and the passive structure of the plasma chamber, based on the currents flowing in the coils. The plasma is followed from shortly after its formation, through the initial current rise phase, and beyond to ignition and burning.

The results show that, when the temporal evolution is considered, stability criteria impose stronger constraints on ignition than the energetics alone. The two are coupled, however, since the evolution of the current density depends on the electron temperature. We find that improved plasma confinement usually also improves the margin that has been built into the Ignitor design against macroscopic plasma instabilities. This is discussed in Sections 4 and 5.

The transport simulations also emphasize the importance of the spatial dependence of the main plasma parameters for ignition. The required values of the global energy and particle confinement times, that are often used as convenient measures of the plasma properties, also depend strongly on the assumptions made about the plasma profiles. An igniting plasma can be dividied into two main regions, an inner region (about half of the radius) where fusion reactions and bremsstrahlung radiation losses become important and an outer region where most of the ohmic heating occurs and that controls the overall diffusion of the current density and the global energy confinement. A thermal transport that permits a narrow, centrally peaked temperature profile, under conditions of strong fusion heating, allows ignition at a lower global energy confinement time than cases where the temperature profile is less peaked. In addition, a peaked temperature profile supports a larger ohmic heating at ignition because there is a large region of low temperature where the ohmic heating remains high. The numerical results provide good examples of these effects [8].

As indicated earlier, a peaked particle density profile is a positive factor in terms of preventing the onset of microinstabilities with relatively long wavelengths that can produce damaging rates of thermal energy transport [10, 11] and is also favorable for ignition. Simulation shows, however, that ignition can be achieved for relatively modest peaking factors, $n_{eo}/\langle n_e\rangle \geqslant 1.5$, under reasonable assumptions on the thermal transport and the formation of well-behaved current density distributions (here $\langle\ \rangle$ indicates the volume average). Based on results from previous experiments at high density, this appears a rather easy requirement to fulfill. As indicated earlier, a pellet injector is considered an integral part of the Ignitor experiment, mainly as a means to ensure that relatively peaked density profiles are produced and maintained.

We note that the phase of constant current ("flat top") after the initial rise is designed to last about 4 sec, at the 12 MA level, with the maximum values of the toroidal field. On the other hand, our analyses indicate that the maximum plasma current and the corresponding (vacuum) toroidal field of 13 T are not necessary to sustain the ignited state. Therefore, by operating at lower currents and fields it is possible to extend the time over which fusion burn conditions can be sustained and the question of assessing whether the accumulation of α-particles may be detectable can be raised. In reality, given the low values of the α-particle density that are obtained by our numerical analysis, it is unlikely that α-particle accumulation effects will be detectable. In addition it should be noted that present experiments with 100% helium plasmas see little recycling of helium from the walls. Therefore helium ash lost through particle transport will compound the difficulty of detecting its rate of accumulation in the plasma column.

We notice also that low temperature ignition is thermally unstable, since the plasma temperature tends to runaway in principle, given the temperature dependence of the fusion reactivity $(\overline{\sigma v})_F$. At the same time, it is not difficult to envision intrinsic plasma processes that may limit the temperature excursion. Among the external means that we intend to employ is the injection of pellets with compositions and sizes chosen in such a way as not to depress the plasma temperature to the point where fusion burning is quenched irreparably.

3.2. *Transport model*

In compact ignition experiments, ohmic heating plays a key role for the evolution of the plasma parameters toward ignition. Therefore, it is important to include, in the numerical model used to simulate the approach to ignition, transport coefficients that, in the regimes where ohmic heating is dominant, reproduce the wealth of experimental observations that are available. In particular, these transport coefficients should:

– Reproduce quantitatively the relevant experimentally estimated confinement times.

– Reproduce the observed temperature profiles and in particular comply with the "principle of profile consistency" [20].

– Comply with the prediction [21], confirmed by a large variety of experiments, that the loop voltage applied to the plasma column under statonary conditions is nearly invariant for all experiments ($V_\phi \simeq 1 \div 1.5$ V).

The Coppi–Mazzucato–Grüber (CMG) diffusion coefficient [21] for the electron thermal energy transport that we adopt has all these features. In Appendix A, a detailed derivation of the Coppi–Mazzucato–Grüber electron thermal diffusion coefficient is given for ohmically heated plasmas, for general axisymmetric geometry [22], based on a particular voltage scaling that fits many experimental plasmas. This form can be written

$$\chi_e^{CMG} \simeq \frac{7.76 \times 10^{11} I_\phi}{n_e^{4/5} T_e} \left(\frac{\ln \Lambda Z_*}{\bar{A}_i}\right)^{2/5} \times \left(\frac{\pi^{3/2} V_a^2}{A_a^{3/2}}\right) \frac{1}{\langle\!\langle |\nabla V|^2 \rangle\!\rangle} \quad (\mathrm{m}^2/\mathrm{sec}), \tag{1}$$

where $\langle\!\langle |\nabla V|^2 \rangle\!\rangle$ is flux surface average of the square of the spatial gradient of the volume V within the surface that contains the toroidal magnetic flux Φ, A_a is the area of the plasma cross section, $\ln \Lambda$ is the Coulomb logarithm, $Z_* = \sum_j n_j Z_j / n_e A_j$ summed over all ions j, $\bar{A}_i$ is the mean ion atomic weight, $I_\phi(\Phi)$ is the toroidal plasma current within Φ, $n_e(\Phi)$ is electron density, and V_a is the total plasma volume. MKS units have been used, except for the electron temperature $T_e = T_e(\Phi)$ in eV.

In the simulations, the effective edge temperature T_{ea} (on the plasma side of the boundary layer connecting the plasma to the limiter or vacuum) has been taken to be an

increasing function of the peak temperature T_{eo}. In particular, we assume that T_{ea} varies from 10 eV for $T_{eo} \leqslant 1$ keV to 400 eV for $T_{eo} \geqslant 4$ keV. Trials with different dependences of the edge temperature on the peak temperature have been carried out and discussed in Ref. [8]. The main results are that larger edge temperatures, during the current rise, slow the current penetration and may allow a hollow current profile to develop, while low edge temperatures give rise to large $q \leqslant 1$ regions earlier in time, due to the rapid current penetration. These results suggest that selective local heating, for instance by an ICRH system, or cooling of the edge region during the current ramp, may be useful to control the current penetration.

When the ohmic heating is no longer dominant, an additional contribution to χ_e is introduced to account for the degradation of confinement that is observed in present-day experiments when an injected heating system is applied. Thus we write the total electron thermal diffusion coefficient as

$$\chi_e = \chi_e^{OH} + \left(\frac{P_\alpha + P_{INJ}}{P_{HEAT}}\right)\chi_e^{UB}, \tag{2}$$

where P_α is the alpha-heating power, P_{INJ} the injected heating power, P_{HEAT} the total input power ($P_{HEAT} = P_\alpha + P_{OH} + P_{INJ}$), P_{OH} being the ohmic heating power, and χ_e^{OH} is an extension of the diffusion coefficient (1) to regimes in which ohmic heating is no longer dominant. In particular we write

$$\chi_e^{OH} = \chi_e^{CMG} \times \left(\frac{V_\phi^*}{V_\phi}\right)^{2/3}, \tag{3}$$

where V_ϕ is the voltage at the edge of the plasma column and V_ϕ^* is the loop voltage that is obtained under steady state conditions when only ohmic heating is applied and that, as indicated earlier and as implied by the CMG coefficient, can vary over a limited range of values. In particular we consider $0.8 < V_\phi^* < 1.6$ (volt) choosing, for a set of parameters typical of Ignitor,

$$V_\phi^* \simeq 0.8\left[1 + \frac{1}{1 + (T_{eo}/2.5)^4}\right] \quad \text{(volt)}, \tag{4}$$

where T_{eo} is in keV.

The chosen form for χ_e^{OH} keeps the total thermal diffusion coefficient χ_e from decreasing, as a function of temperature, in the transition regime between ohmic and fusion dominated heating (Fig. 6, Section 4.1). The degradation of τ_E near ignition is modeled by the thermal transport coefficient that describes injected heating regimes.

The additional diffusion coefficient χ_e^{UB} that appears in eq. (2) has been derived by the criteria that it:

(*i*) Reproduce the class of electron temperature profiles that are commonly observed in the experiments.

(*ii*) Give a scaling for the energy confinement time that is consistent with a relatively large variety of experiments [6]. It should be noted, however, that these experiments do not include high density and high magnetic field regimes which, whenever they have been produced, have demonstrated superior confinement properties.

(*iii*) Theoretically is based on a combination of the effects of the trapped electron "ubiquitous" mode [23] and the collisional impurity driven mode [24]. The latter mode is assumed to be excited in the outer region of the column [25] and the former in the main body of it.

In particular

$$\chi_e^{UB} = C_{UB}\left(\frac{8}{\mu_o e n_e(\Phi)}\frac{dp(\Phi)}{dI_\phi(\Phi)}\right)^2 \times \frac{1}{q(\Phi)Rv_{the}}\frac{Z_{eff}^{1/2}}{A_i}(ar_*)\left(\frac{r_*}{R}\right)^{1/2} \quad (\mathrm{m}^2/\mathrm{sec}), \tag{5}$$

where $p(\Phi)$ is the total plasma pressure, $v_{the} = (2T_e/m_e)^{1/2}$ the electron thermal velocity, R the major radius, $q(\Phi)$ the magnetic field line parameter, a the average minor radius, $r_* = r + a/10$, where r is the minor radius. The approximate distance r_* has been introduced in order to extend the diffusion coefficient to the center of the plasma column. The numerical coefficient C_{UB} is evaluated in such a way that the total energy confinement time τ_E reproduces present day experiments with injected heating [6, 26] in the so-called L-mode, as described later.

The diffusion coefficient χ_i for the ion thermal energy is taken to be a combination of the collisional (so-called neoclassical) diffusion coefficient [27] and one resulting from the excitation of collective modes. In particular, we assume that the formation of flat density profiles can be prevented by the use of a pellet injector if necessary, as in the case of the Alcator–C experiments. Therefore, we exclude [11] the contribution to χ_i of the so-called η_i-mode, where $\eta_i \equiv \mathrm{d}\ln T_i/\mathrm{d}\ln n$. Instead we include the contribution of the same modes that produce the diffusion coefficient χ_e^{UB}, as

$$\chi_i = \chi_i^{NEO} + \gamma_i\left(\frac{P_\alpha + P_{INJ}}{P_{HEAT}}\right)\chi_e^{UB}, \tag{6}$$

where γ_i is a numerical coefficient that, given the considered values of η_i, we can safely assume to be less than unity ($\gamma_i = 0.5$ is our reference value). It is clear that if $T_i \simeq T_e$ the scaling of the energy confinement time can give a numerical value for $C_{UB}(1 + \gamma_i)$. In particular we may take $C_{UB} \approx 1$ as a plausible numerical value that reproduces the Lackner–Gottardi scaling [6] for the L-mode, when the electrons dominate the thermal losses ($\gamma_i = 0.5$) and χ_e^{UB} is written as

$$\chi_e^{UB} \simeq C_{UB}\left(\frac{4\times 10^{25}}{n_e(\Phi)}\frac{dp}{dI_\phi}\right)^2 \times \frac{1}{q(\Phi)Rv_{the}}\frac{Z_{eff}^{1/2}}{A_i}(ar_*)\left(\frac{r_*}{R}\right)^{1/2} \quad (\mathrm{m}^2/\mathrm{sec}). \tag{7}$$

where the MKS unit system is used.

We point out that it is inappropriate and overly pessimistic to compare the assessed values of the energy confinement time for Ignitor (e.g., Figs 7 and 9c, Section 4.1) with the so-called "empirical" scalings obtained from the L-mode of operation. In this regime the rate of ohmic heating is negligible relative to that of injected heating, a circumstance that does not occur in the case of Ignitor, where in addition all the heating is internal, and a complete degradation of confinement should not be expected.

The latest scaling for the energy confinement time obtained for the H-regime from the results of three advanced experiments has been given in Ref. [28]. We note that the range of plasma densities for which this scaling has been obtained is quite limited and well below the densities

at which Ignitor is designed to operate. Therefore a favorable effect of high density operation is not included in this scaling, that is written as

$$\tau_E \simeq 0.11 I_p^{1.08} P_L^{-0.49} R_0^{1.45} \quad \text{(sec, MA, MW, m)}.$$

We also note that higher values of τ_E than predicted by this scaling have been obtained recently by the DIII-D experimental facility [29]. The scalings proposed by Lackner–Gottardi [6] and by Coppi [26], while providing a comparable fit to the experiments where P_{INJ} is prevalent, can be traced back to the effects of trapped electrons. In particular, the Coppi scaling is related to the theory of the collisionless trapped electron mode (so-called "ubiquitous"), i.e. to eq. (5), and is

$$\tau_E \simeq 1.75 \times 10^{-13} \left(\frac{\bar{n}_e \kappa}{P_{INJ}}\right)^{0.6} \left(\frac{I_P}{\alpha_T}\right)^{0.8} \times a R_0^{1.2} (q_\psi \bar{A}_i)^{0.4} Z_{eff}^{-0.2} \quad \text{(sec)},$$

where, $\bar{n}_e$ is the line averaged electron density, κ the elongation of the plasma cross section and α_T is the temperature profile factor [$\alpha_T = -\mathrm{d} \ln T/\mathrm{d}(r/a)^2$ in circular geometry].

The plasma current density is assumed to be locally related to the applied electric field by the collisional electrical resistivity $\eta_\parallel$ (so-called neoclassical) [30] that includes the effects of the presence of a relatively large population of trapped electrons. Although this assumption is commonly made, we have argued [7] that the detailed evolution of the current density profile should include additional processes. In fact, we intend to adopt the current density transport equation proposed in Ref. [7] as a replacement for the simple Ohm's law, in a future continuation of the present work.

We have also carried out extensive numerical simulations of the approach to ignition using a simplified model of χ_e that includes a degradation factor, intended to represent the possible effect of α-particle heating, given by [8]

$$\chi_e = \chi_e^{CMG} \left[1 + \gamma_e \beta_p \left(\frac{P_\alpha + P_{INJ}}{P_{HEAT}}\right)\right] f\left(\frac{T_{eo}}{T_{OH}}\right). \tag{8}$$

Here γ_e is a degradation numerical coefficient chosen in such a way that the confinement time typical of the so-called L-mode can be obtained, $\beta_p = 4\langle n_e T_e + \sum_j n_j T_j\rangle/\mu_o R_o I_p^2$ and $f(T/T_{OH}) = 1$ for $T < T_{OH}$ and T/T_{OH} for $T \geqslant T_{OH}$, where T_{OH} is a reference temperature above which the confinement is expected to degrade (typically, we choose 5 keV for Ignitor to reproduce the onset of the degradation observed in typical L-mode scalings for the energy confinement time).

Finally, we observe that the question of the particle transport in an ignition experiment has received relatively little attention up to the present, despite the importance of the density profiles to ignition. In our case we have started our analysis of free boundary configurations by assuming that specified density profiles of the main ion species and impurities can be maintained. Recycling from the walls and energy losses due to ionization and charge exchange have been neglected. In fact, our preliminary results from a fixed boundary transport code (BALDUR) [31] show that recycling from the walls produces a significant density of neutral deuterium and tritium only in the outer few centimeters of the plasma. We point out that we have developed both analytical [32] and numerical models to describe the anomalous particle transport including both outward diffusion and inward flow. On the basis of our previous experience with these models we do not expect a significant change in the conditions under which ignition conditions can be achieved, relative to the cases where appropriate fixed density profiles are assumed for simplicity.

4. Numerical results

4.1. *Energy requirements*

Ignition is defined to occur when

$$P_\alpha = P_L,$$

P_α being the fusion heating due to alpha particles, and P_L the total power lost by radiation, conduction, etc. Therefore at this point the thermal stored energy of the plasma is increasing as

$$\frac{\mathrm{d}W}{\mathrm{d}t} = P_H,$$

where $P_H = P_{OH} + P_{INJ}$ is the nonfusion power source. The energy confinement time is

$$\tau_{E,IGN} = \frac{W_{IGN}}{P_{L,IGN}}.$$

If we represent the low temperature approximation to the fusion reactivity by $(\overline{\sigma v})_F \propto T^{\alpha_F}$ where $\alpha_F \gtrsim 2$, then we obtain the well-known condition

$$\tau_{E,IGN} \propto \frac{1}{n_o T_o^{\alpha_F - 1}} Q_p,$$

where the factor Q_p represents the effects of the plasma radial profiles.

The numerical results show that ignition in compact experiments can be achieved at record low temperatures where ohmic heating is still important and the energy confinement time is not yet strongly degraded. For the Ignitor parameters given in Table I, ignition can be reached at $T_o \simeq 11$ keV and $n_{eo} \simeq 1.1 \times 10^{21}\, m^{-3}$, corresponding to a thermal stored energy $W_{IGN} \simeq 12$ MJ. If the peaking of the temperature profile $T_{eo}/\langle T_e\rangle \simeq T_{io}/\langle T_i\rangle$ is limited to approximately 3, then $\tau_{E,IGN} \simeq 660$ msec when $Z_{eff} \simeq 1.2$, as shown in Table II. We notice also that P_α in this case is about 18 MW and this makes the thermal loading of the first wall relatively mild. Another advantage of early ignition is that this occurs when the volume contained within the surface $q = 1$ is less than 1/10 of the total plasma volume. This keeps the effects of potential sawtooth oscillations small and also makes them easier to stabilize, as discussed in Section 4.2.

The initial current ramp phase, during which the magnetic field, density, and plasma size are also increased, has been shown to have several important features for a compact ignition experiment [7, 8]. First, the ohmic heating

Table II. *Reference discharge*

	Start	End of ramp	Ignition
t (sec)	0.2	3.0	4.3
R_o (m)	1.07	1.3	1.3
a (m)	0.26	0.47	0.47
κ	1.07	1.87	1.87
δ_G	0.08	0.42	0.43
$l_i/2$	0.47	0.32	0.36
β_p	—	0.08	0.13
β (%)	0.06	0.8	1.26
β_α (%)	—	0.005	0.12
$n_{eo}^{\dagger}$ (10^{20} m^{-3})	2.5	11.0	11.0
$n_{\alpha o}$ (10^{17} m^{-3})	—	1.5	12.0
q_o	1.75	0.83	0.71
q_ψ	4.2	3.3	3.6
$Vol_{q<1}$ (%)	—	1.4	5.8
I_p (MA)	0.95	12.0	12.0
W_{int} (MJ)	0.07	7.5	11.7
T_{eo} (keV)	1.1	4.0	11.0
τ_E (msec)	130	710	660
P_{OH} (MW)	1.5	13.0	9.5
P_α (MW)	—	2.0	17.8
P_B (MW)	0.02	3.2	4.1
P_{IC} (MW)	0.01	0.4	0.5
V-s(V sec)	2.0	29.2	31.4
I_{BS} (MA)	—	0.6	1.0
P_L/S_0 (MW/m^2)	—	0.2	0.4

† Density raised according to Fig. 4

ncreases continuously during the current rise, when the plasma density is also increased (shown in Fig. 2 for a ypical ignition sequence); the increase is linear in time at constant dI_p/dt and dn_e/dt. Relatively large values of P_{OH} can be obtained even when central temperatures approach gnition levels, the reason being that, under nonstationary conditions, the loop voltage is a strong function of the plasma radius and is much higher at the edge than in the center (see Fig. 3). The current ramp drives a broad current density profile, which generates the maximum ohmic heating power density well away from the magnetic axis typically, around $r \simeq a/2$ during the ramp phase), where the emperature is relatively low. After the current ramp ends, he total ohmic heating falls gradually as the overall temperature rises, although not as quickly as the central voltage $V_{\phi o} \propto T_{eo}^{-3/2}$. Increasing the plasma density helps to keep he temperature low in the outer part of the plasma, a condition favorable for ohmic heating. Thus broader density profiles are more favorable for ohmic heating, although not or ignition (see Table 4).

A representative ignition sequence that illustrates these haracteristics is shown in Figs 2–7 and in Table II. Figure 2 shows the volume integrated powers and central temperature as a function of time, while Fig. 4 shows the prescribed total plasma current and particle density. Figure 5 hows profiles of the toroidal current density J_ϕ at representative times. A standard current and density ramp is considered, lasting 3 seconds to a final current $I_p \simeq 12$ MA, $B_T \simeq 13$ T, and $n_{eo} \simeq 1.1 \times 10^{21}$ m^{-3}, with the ratio of central to volume average density $n_{eo}/\langle n_e \rangle \simeq 2.2$ and $n_{ea}/n_{eo} \simeq 0.1$, n_{ea} being the edge density. The transport models represented by eqs (1)–(7) with the coefficients $\chi_{UB} \simeq 1$ and $\gamma_i \simeq 0.5$ were used. The simulation was started at $t \simeq 0.2$ sec after the plasma initiation, with a small circular plasma on the small major radius side of the torus and

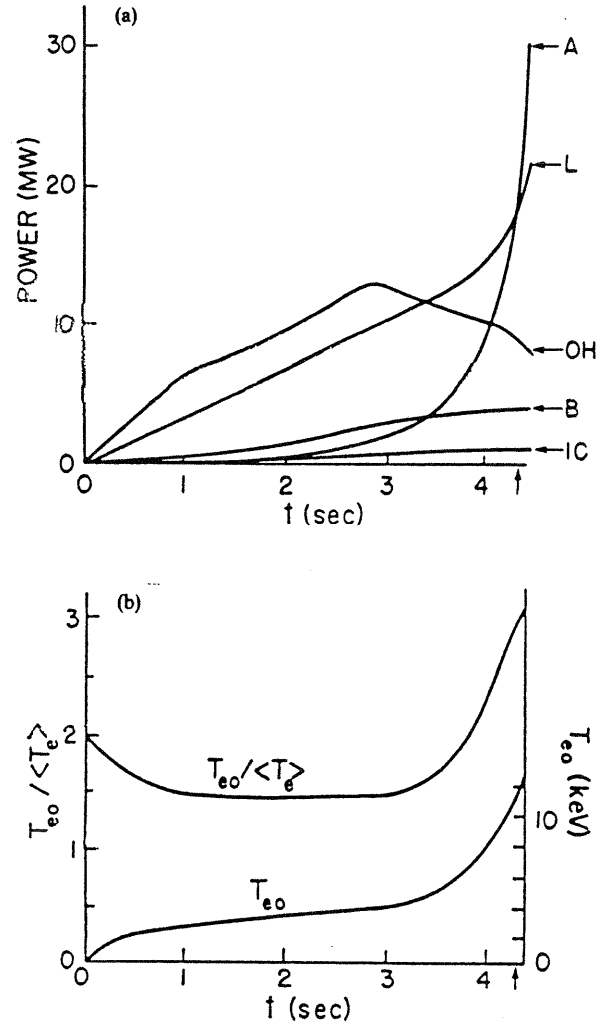

Fig. 2. Time evolution of a representative Ignitor discharge showing a 3 second current ramp and part of the current flat top at $I_p \simeq 12$ MA, $B_T \simeq 13$ T, $n_{eo} \simeq 1.1 \times 10^{21}$ m^{-3}. Ignition occurs at 4.3 sec, marked by an arrow. Volume integrated powers are shown in (a) and central central temperature ($T_{eo} \simeq T_{io}$) in (b). The heating powers are labelled as: OH, ohmic heating; A, α-heating; and the thermal losses by L, total Losses, including conduction; B, bremsstrahlung radiation; IC, cyclotron and carbon impurity radiation ($Z_{eff} \simeq 1.2$). The plasma current, size, and density are increased rapidly until $t \simeq 1$ sec, then more slowly to their final values at $t = 3$ sec as shown in Fig. 4. Initial conditions and parameters are given in Table II

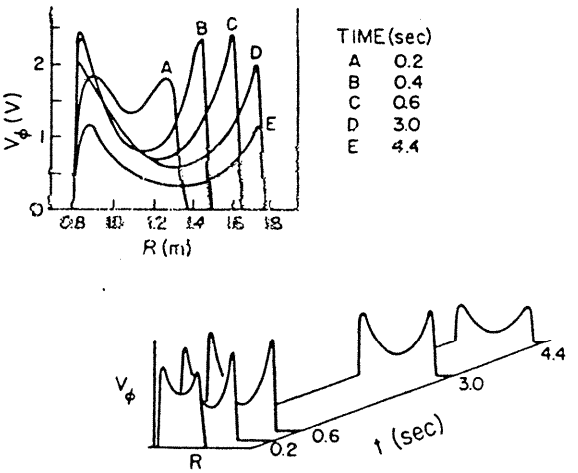

Fig. 3. Time evolution of the loop voltage, as a function of the plasma radius, for the reference discharge of Table II

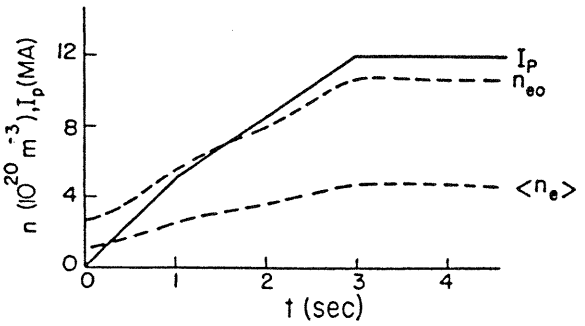

Fig. 4. Time evolution of the plasma current and the particle (electron) density for the case of Table II. The central and volume average values of the density are shown

relatively high values of q ($q_o \simeq 1.8$, $q_\psi \simeq 4.2$). The initial vacuum magnetic field was $B_{T_o} \simeq 8.5\,\mathrm{T}$ at $R_o = 1.3\,\mathrm{m}$, with an assumed current of 1 MA, a peak density $n_{eo} \simeq 2.5 \times 10^{20}\,\mathrm{m}^{-3}$, and a temperature $T_{eo} \simeq 1\,\mathrm{keV}$. The plasma Z_{eff} was assumed to be 1.2, with a carbon impurity and equal amounts of deuterium and tritium. The current was ramped at a faster rate, 5 MA/sec, for the first second (until $t \simeq 1$ sec), then at a slower, constant rate until the end of the ramp ($t = t_R = 3$ sec) (see Fig. 4). We note that these rates of current rise are slower than those that can be estimated from the rates of current rise practiced in the JET experiments, assuming that the current penetrates by a resistive diffusion process. Ignition occurs at $t \simeq 4.3$ sec (Fig. 6), with $dW/dt > 0$, at a central temperature of $T_{eo} \simeq T_{io} \simeq 11\,\mathrm{keV}$, $P_\alpha \simeq 18\,\mathrm{MW}$, $P_{OH} \simeq 9.5\,\mathrm{MW}$, bremsstrahlung radiation loss $P_B \simeq 4\,\mathrm{MW}$, and combined impurity and cyclotron radiation losses $P_{IC} \simeq 0.5\,\mathrm{MW}$. As already mentioned, this level of power at ignition makes the thermal loading on the first wall relatively mild.

The energy confinement time is compared to the predictions of various "empirically" suggested scalings [6, 26, 33–36) in Fig. 7, although as we pointed out in Section 3 the scalings do not really apply and are overly pessimistic for the regimes that are characteristic of Ignitor. Thermal transport models valid for ohmic heating, described in Section 3.2, predict that the energy confinement time at the end of the (primarily ohmic) current ramp in Ignitor is $\tau_E \simeq$ 700 msec (for the standard 3 sec ramp to $I_p \simeq 12\,\mathrm{MA}$ with $n_{eo} \simeq 1.1 \times 10^{21}\,\mathrm{m}^{-3}$). The crucial question for ignition is

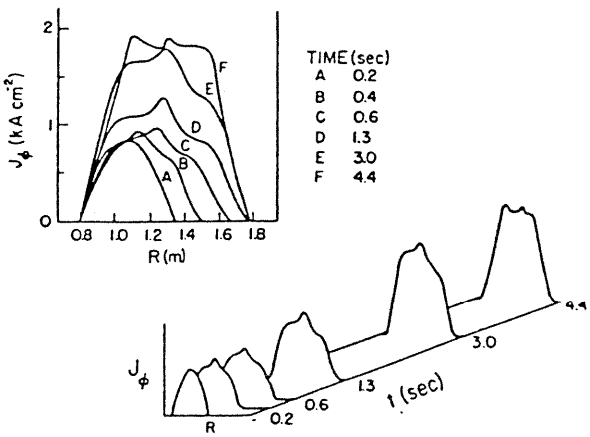

Fig. 5. Time evolution of the toroidal current density profile for the reference case of Table II, as functions of the plasma radius

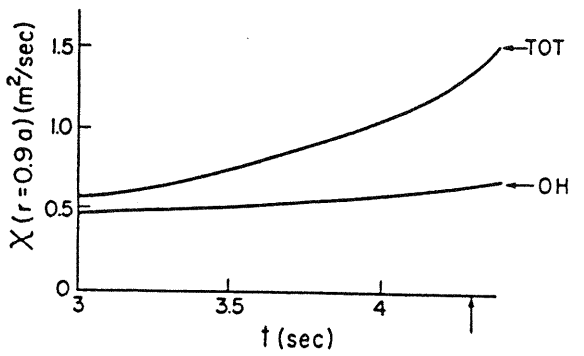

Fig. 6. Total electron and ion thermal diffusion coefficient and ohmic electron thermal diffusion coefficient, evaluated at $r = 0.9a$ on the horizontal midplane, as a function of time during the flat top part of the discharge, for the reference case of Table II. Ignition, marked by an arrow, occurs at 4.3 sec. The total χ is obtained for $C_{UB} = 1$, $\gamma_i = 0.5$ and χ_e^{OH} as defined by eqs 3 and 5

how fast the confinement degrades from ohmic as the fusion heating becomes important. If τ_E does not drop significantly below the level reached at the end of the ramp, when the fusion power becomes important, ignition with ohmic heating alone occurs easily. In this regard, we note that the confinement scalings shown in Fig. 7 represent an arbitrary combination, with the form $1/\tau_E = (\tau_{NA}^{-2} + \tau_{INJ}^{-2})^{1/2}$, of an ohmic scaling (neo-Alcator) and one derived from experiments completely dominated by injected heating in the L-mode regime. This combination predicts a total τ_E that is down by a factor of $1/\sqrt{2}$ from either scaling alone, when the two are equal. (The ohmic neo-Alcator scaling τ_{NA} is also shown in Fig. 7 for comparison.)

The effects of different degrees of degradation, obtained by increasing the ion thermal transport or the effective charge Z_{eff}, are shown in Table III. The ion anomalous thermal transport loss enhanced by a factor of 2 over the

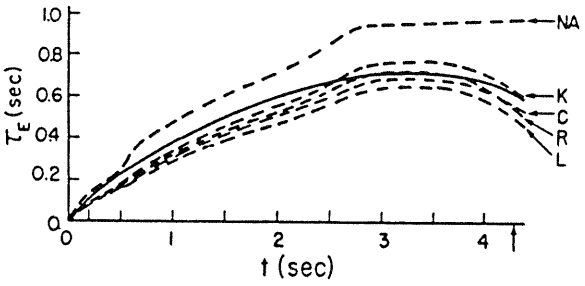

Fig. 7. Energy confinement time for the case of Figs 2–6 (solid curve), compared to the estimates made from various global scalings (broken curves). In our simulation τ_E decreases as P_α exceeds P_{OH}, when the non-ohmic heating transport becomes dominant. The scalings are: NA, neo-Alcator $\tau_{NA} = 0.07 \bar{n}_e R^2 a q_*$, where $\bar{n}_e$ in $10^{20}\,\mathrm{m}^{-3}$ and

$$q_* \equiv \left(\frac{5a^2 B_T}{R_o I_p}\right) \frac{[1 + \kappa^2(1 + 2\delta^2 - 1.2\delta^3)]}{2},$$

B_T(T), I_p (MA); R, Rebut–Lallia [32]; K, Kaye All–Complex [33]; C, Coppi [26]; and L, Lackner–Gottardi [6]. These last 4 scalings are combinations of τ_{NA} and the L-mode scalings found for plasmas dominated by injected heating, $1/\tau_E = (\tau_{NA}^{-2} + \tau_{INJ}^{-2})^{1/2}$. We point out that it is inappropriate and overly pessimistic to compare the assessed values of the energy confinement time for Ignitor with the so-called "empirical" scalings obtained from the L-mode of operation. In this regime the rate of ohmic heating is negligible relative to that of injected heating, a circumstance that does not occur in the case of Ignitor, where all forms of heating are internal and a complete degradation of confinement should not be expected

Table III. *Degraded discharges*

	Reference discharge	Larger ion transport†	Still larger ion transport†*	Larger Z_{eff}
γ_i	0.5	1.0	1.5	0.5
Z_{eff}	1.2	1.2	1.2	1.6
t_{ign} (sec)	4.3	4.6	5.0*	5.2
β_p	0.13	0.14	0.14	0.14
W_{int} (MJ)	11.7	13.0	12.9	12.8
T_{eo} (keV)	11.0	12.9	13.4	13.0
τ_E (msec)	660	540	470	570
P_{OH} (MW)	9.5	8.4	8.1	8.7
P_α (MW)	17.8	24.0	24.3	22.5
P_B (MW)	4.1	4.2	4.2	4.9
P_{IC} (MW)	0.5	0.5	0.5	1.0
$Vol_{q=1}$ (%)	5.8	>10	>10	>10
$T_{q=1}$ (keV)	—	8.4	6.3	5.0

* Sub-ignited plasma with $P_\alpha/P_L \simeq 0.8$ and $W \simeq 4.9$ MW
† χ_i^{an} has little effect during the current ramp (ohmic)

reference case (by increasing γ_i to 1.0), results in a marginally ignited plasma, as does increasing Z_{eff} from 1.2 to around 1.6. In the case of Table III, the ion anomalous thermal transport has relatively little effect during the current ramp, which remains dominated by ohmic heating. The major effect of increased Z_{eff} is the dilution of the fusion nuclei and larger bremsstrahlung radiation losses that lead to reduced central heating, an effect that is partially compensated by a larger ohmic heating ($P_{OH} \simeq 14.5$ MW at the end of the ramp for $Z_{eff} \simeq 1.6$ while for the reference discharge $P_{OH} \simeq 13$ MW).

Broadening the density profile from $n_o/\langle n\rangle \simeq 2.2$ to 1.5 at the same peak density increases the ohmic heating and the bremsstrahlung radiation loss P_B, but still allows ignition at slightly higher τ_E, although with a larger region where $q < 1$. Narrowing the density profile from $n_o/\langle n\rangle \simeq 2.2$ to 2.9 produces only small improvements in the ignition time and the size of the region where $q \leqslant 1$, but allows ignition at smaller values of τ_E (see Table IV and Fig. 8 where $n_o/\langle n\rangle$ is varied at constant n_o). Figure 8(*a*) shows the variation in the ignition time and the size of the $q \leqslant 1$ region with density peaking, while Fig. 8(*b*) shows the energy confinement time at ignition.

The effects of changing the peak plasma density n_o at the end of the current ramp or during the flat top phase of the discharge are shown in Tables V–VII, respectively, for different levels of degradation. The lower peak densities around

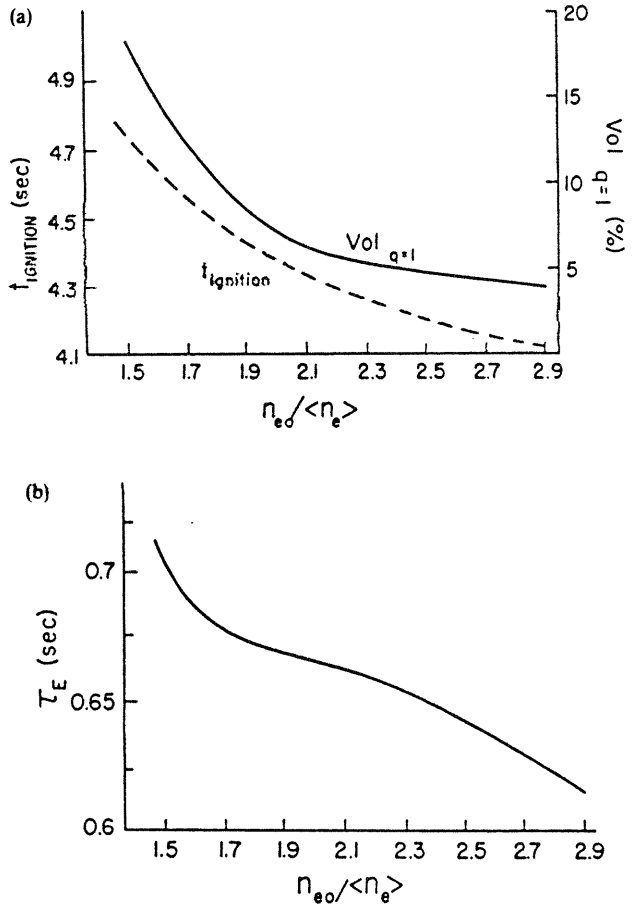

Fig. 8. Ignition time t_{ign} (broken curve) and volume $Vol_{q=1}$ inside the surface where $q = 1$ at ignition are shown in (*a*) and the necessary energy replacement time in (*b*), as a function of the shape of the density profile ($n_o/\langle n\rangle$) for fixed electron peak density ($n_{eo} \simeq 1.1 \times 10^{21}\, m^{-3}$). All these parameters decrease as the electron density profiles become more peaked. Initial conditions and current ramp are the same as for the reference case of Table II

$0.9 \times 10^{21}\,m^{-3}$ ignite in a shorter time than densities $n_o \simeq 1.1 \times 10^{21}\,m^{-3}$ with the reference transport model (see Table V). On the other hand the larger peak densities become more attractive when τ_E is degraded ($\gamma_i = 1 \div 1.5$) as they allow ignition at lower peak plasma temperature and lower levels of α-power (see Tables VI and VII).

Too large a peak density may produce hollow temperature profiles during the current ramp, introducing a delay in the α-power production. Better results, in terms of

Table IV. *Effects of different density profiles*†

	Broad profile	Reference profile	Narrow profile
$n_{eo}/\langle n_e\rangle$	1.5	2.2	2.9
t_{ign} (sec)	4.7	4.3	4.1
β_p	0.15	0.13	0.12
W_{int} (MJ)	13.4	11.7	10.7
T_{eo} (keV)	11.1	11.0	11.2
τ_E (msec)	705	660	615
P_{OH} (MW)	9.9	9.5	8.8
P_α (MW)	19.0	17.8	17.4
P_B (MW)	5.8	4.1	3.2
P_{IC} (MW)	0.8	0.5	0.4
$Vol_{q=1}$ (%)	>10	5.8	4.0
$T_{q=1}$ (keV)	6.5	—	—

† At the same peak density $n_{eo} \simeq 11.0 \times 10^{20}\,m^{-3}$

Table V. *Effects of different n_o† on the reference discharge*

	Lower peak density	Reference density	Larger peak density
n_{eo} ($10^{20}\,m^{-3}$)	9.0	11.0	13.0
t_{ign} (sec)	4.1	4.3	4.7
W_{int} (MJ)	11.5	11.7	12.3
T_{eo} (keV)	13.5	11.0	9.8
τ_E (msec)	590	660	670
P_{OH} (MW)	8.3	9.5	10.1
P_α (MW)	19.5	17.8	18.3
P_B (MW)	3.0	4.1	5.3
P_{IC} (MW)	0.5	0.5	0.5
$Vol_{q=1}$ (%)	4.0	5.8	>10
$T_{q=1}$ (keV)	—	—	6.6

† At the same density profile $n_{eo}/\langle n_e\rangle = 2.2$

Table VI. *Effects of different* n_o† *on a degraded discharge* ($\gamma_i = 1.0$)

	Lower peak density	Reference density	Larger peak density
n_{eo} (10^{20} m^{-3})	9.0	11.0	13.0
t_{ign} (sec)	5.0*	4.6	4.9
W_{int} (MJ)	12.6	13.0	12.7
T_{eo} (keV)	15.7	12.9	10.7
τ_E (msec)	410	540	610
P_{OH} (MW)	7.0	8.4	9.7
P_α (MW)	24.0	24.0	20.9
P_B (MW)	3.1	4.2	5.3
P_{IC} (MW)	0.6	0.5	0.5
$T_{q=1}$ (keV)	11.0	8.4	5.5

† At the same density profile $n_{eo}/\langle n_e \rangle \simeq 2.2$
* Sub-ignited plasma with $P_\alpha/P_L \simeq 0.8$ and $W \simeq 0.4$ MW

shorter ignition time and better stability against $m^o = 1$ modes, are obtained by limiting the peak density to the reference values during the current ramp and increasing, if needed, its value during the flat top (see Table VIII). In the numerical simulations reported in Tables VII and VIII the rate of change of the peak electron density is chosen in such a way that, keeping it constant during the flat top, the final value of the plasma density is well within the density limits estimated from present day experiments.

An example of a limiting case that does not quite reach ignition, but eventually settles into a state of sustained, sub-ignited burning at moderate levels of fusion power, is shown in Fig. 9 and Table III, case 3. The parameters are similar to those of the reference case of Figs 2–7, except for an artificially increased ion thermal transport, $\gamma_i = 1.5$. Figure 9 shows the power balance, the central temperature, that in the sub-ignited burning state is $T_o \simeq 11.6$ keV, and τ_E. Figure 9(*c*) shows that this level of ion transport exceeds predicted L-mode levels even during the α-heating stage.

A few MW of injected heating, started during the current ramp, aid substantially in shortening the time to ignition and in controlling the size of the $q \leqslant 1$ region (see Tables IX–XII). The increased central heating shortens the ignition interval, while the higher temperature in the outer half of the plasma slows the rate of current penetration so that the central q drops more slowly. High temperatures in the

Table VII. *Effects of increasing the peak density during the flat top*

	Reference transport		Larger transport		Still larger transport	
$\dot{n}_{eo}$ (10^{20} m^{-3} sec^{-1})	—	1.7	—	1.7	—	1.7
n_{eo}† (10^{20} m^{-3})	11.0	13.8	11.0	14.0	11.0	14.5
γ_i	0.5	0.5	1.0	1.0	1.5	1.5
t_{ign} (sec)	4.3	4.5	4.6	4.7	5.0*	5.0
β_p	0.13	0.14	0.14	0.15	0.14	0.16
W_{int} (MJ)	11.7	12.4	13.0	13.0	12.9	14.1
T_{eo} (keV)	11.0	9.2	12.9	9.9	13.4	10.7
τ_E (msec)	660	705	540	635	470	545
P_{OH} (MW)	9.5	10.4	8.4	10.2	8.1	9.6
P_α (MW)	17.8	17.6	24.0	20.5	24.3	25.8
P_B (MW)	4.1	5.9	4.2	6.0	4.2	6.8
P_{IC} (MW)	0.5	0.6	0.5	0.6	0.5	0.7
$Vol_{q=1}$ (%)	5.8	>10	>10	>10	>10	>10
$T_{q=1}$ (keV)	—	6.2	8.4	5.2	6.3	4.8

* Sub-ignited plasma with $P_\alpha/P_L \simeq 0.8$ and $W \simeq 2.6$ MW
† Value at ignition

Table VIII. *Large density discharges with* $\dot{n}_{eo} = 0$ *or* $\dot{n}_{eo} \neq 0$ *during the flat top*

	Reference transport		Larger transport		Still larger transport	
n_{eo}‡ (10^{20} m^{-3})	13.8	11.0	14.0	11.0	14.5	11.0
$\dot{n}_{eo}$ (10^{20} m^{-3} sec^{-1})	—	1.7	—	1.7	—	1.7
n_{eo}† (10^{20} m^{-3})	13.8	13.8	14.0	14.0	14.5	14.5
γ_i	0.5	0.5	1.0	1.0	1.5	1.5
t_{ign} (sec)	5.0	4.5	5.2	4.7	5.8	5.0
β_p	0.14	0.14	0.14	0.15	0.17	0.16
W_{int} (MJ)	12.5	12.4	13.0	13.0	14.9	14.1
T_{eo} (keV)	9.5	9.2	10.3	9.9	12.3	10.7
τ_E (msec)	680	705	605	635	470	545
P_{OH} (MW)	10.3	10.4	10.1	10.2	8.6	9.6
P_α (MW)	18.4	17.6	21.3	20.5	31.8	25.8
P_B (MW)	5.7	5.9	5.9	6.0	6.6	6.8
P_{IC} (MW)	0.6	0.6	0.6	0.6	0.7	0.7
$T_{q=1}$ (keV)	4.5	6.2	3.9	5.2	3.2	4.8

* Sub-ignited plasma with $P_\alpha/P_L \simeq 0.8$ and $W \simeq 2.6$ MW
† Value at ignition
‡ Value at the beginning of the flat top

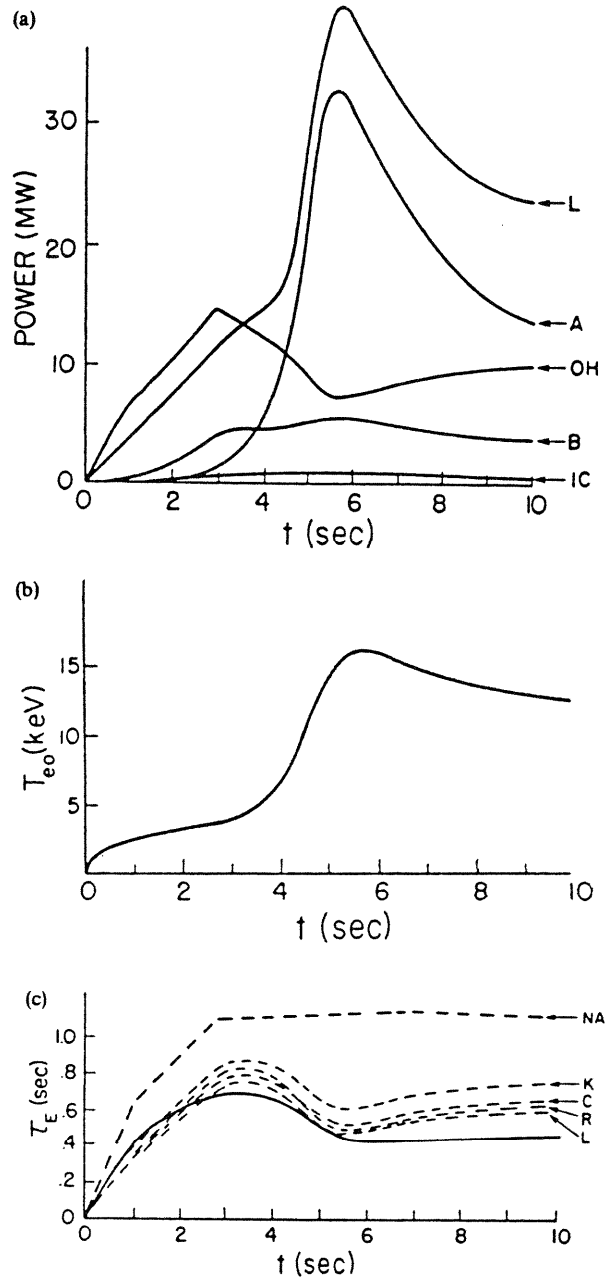

Fig. 9. Time evolution of an Ignitor plasma with enhanced ion thermal transport ($\gamma_i = 1.5$). Initial parameters and current ramp are the same as for the reference case of Table II. Ignition is not reached in the absence of an injected heating system, and the plasma approaches a sub-ignited steady state. The quenching that occurs after a peak ion temperature of about 12 keV is achieved, can be viewed as a response to the increased rate of transport that follows the temperature rise, while the ohmic heating is decreasing. Volume integrated powers are shown in (*a*), central temperature in (*b*) and energy confinement time compared to various scalings in (*c*). Labels are the same as in Figs 2 and 7

central region, $T_{eo} \gtrsim 10$ keV, act to "freeze in" the central current density. Table IX illustrates the effects of ICRH heating on the reference case and one of the two degraded cases of Table III ($\gamma_i = 1.5$) when up to 15 MW of ICRH is applied starting at $t \simeq 1.2$ sec ($P_{INJ} = 5$ MW for $1.2 < t < 1.8$ sec, 10 MW for $1.8 < t < 2.4$ sec, and 15 MW for $t > 2.4$ sec). These cases ignite before the end of the ramp (note that densities and currents are below the flat top levels). Tables X and XI report the effects of different levels of injected heating on the reference discharge and on the

Table IX. *Effects of ICRH heating on reference and degraded discharges*

	Reference transport		Larger transport	
P_{INJ} (MW)	—	15.0†	—	15.0†
γ_i	0.5	0.5	1.5	1.5
I_p	12.0	10.6**	12.0	12.0
n_{eo} (10^{20} m^{-3})	11.0	9.5**	11.0	11.0
t_{ign} (sec)	4.3	2.5	5.0*	3.0
β_p	0.13	0.18	0.14	0.19
W_{int} (MJ)	11.7	12.4	12.9	16.6
T_{eo} (keV)	11.0	12.5	13.4	15.1
τ_E (msec)	660	530	470	425
P_{OH} (MW)	9.5	6.7	8.1	6.9
P_α (MW)	17.8	23.3	24.3	39.2
P_B (MW)	4.1	3.2	4.2	4.9
P_{IC} (MW)	0.5	0.4	0.5	0.7
$Vol_{q=1}$ (%)	5.8	0.5	>10	1.4
$T_{q=1}$ (keV)	—	—	6.3	—

* Sub-ignited plasma with $P_\alpha/P_L \simeq 0.8$ and $W \simeq 4.9$ MW
** Lower values due to ignition during ramp
† $P_{INJ} \simeq 5$ MW for $1.2 < t < 1.8$ sec, 10 MW for $1.8 < t < 2.4$ sec, and 15 MW for $t > 2.4$ sec

Table X. *Effects of different level of ICRH heating on the reference discharge*

	Ohmic discharge	Low P_{INJ}	Large P_{INJ}
P_{INJ} (MW)	—	5.0‡	15.0†
I_p (MA)	12.0	11.8**	10.6**
n_{eo} (10^{20} m^{-3})	11.0	10.8**	9.5**
t_{ign} (sec)	4.3	2.9	2.5
β_p	0.13	0.14	0.18
W_{int} (MJ)	11.7	11.8	12.4
T_{eo} (keV)	11.0	11.0	12.5
τ_E (msec)	660	650	530
P_{OH} (MW)	9.5	9.3	6.7
P_α (MW)	17.8	18.2	23.3
P_B (MW)	4.1	3.9	3.2
P_{IC} (MW)	0.5	0.4	0.4
$Vol_{q=1}$ (%)	5.8	1.4	0.5

† $P_{INJ} \simeq 5$ MW for $1.2 < t < 1.8$ sec, 10 MW for $1.8 < t < 2.4$ sec, and 15 MW for $t > 2.4$ sec
‡ $P_{INJ} \simeq 5$ MW for $t > 1.2$ sec
** Lower values due to ignition during the ramp

Table XI. *Effects of different level of ICRH heating on a degraded case ($Z_{eff} = 1.6$)*

	Ohmic discharge	Low P_{INJ}	Large P_{INJ}
P_{INJ} (MW)	—	5.0†	15.0‡
Z_{eff}	1.6	1.6	1.6
I_p (MA)	12.0	12.0	11.2*
n_{eo} (10^{20} m^{-3})	11.0	11.0	10.0*
t_{ign} (sec)	5.3	3.3	2.7
β_p	0.14	0.15	0.18
W_{int} (MJ)	12.8	14.0	13.6
T_{eo} (keV)	13.0	13.2	13.4
τ_E (msec)	570	555	525
P_{OH}	8.7	8.8	7.2
P_α (MW)	22.5	25.2	25.9
P_B (MW)	4.9	5.4	4.4
P_{IC} (MW)	1.0	1.1	1.0
$Vol_{q=1}$ (%)	>10	2.3	0.5
$T_{q=1}$ (keV)	5.0	—	—

* Lower values due to ignition during the ramp
† $P_{INJ} \simeq 5$ MW for $t > 1.2$ sec
‡ $P_{INJ} \simeq 5$ MW for $1.2 < t < 1.8$ sec, 10 MW for $1.8 < t < 2.4$ sec, and 15 MW for $t > 2.4$ sec

Table XII. *Marginally ignited plasmas with ICRH heating*

	Large ion transport	Large Z_{eff}
P_{INJ} (MW)	15.0‡	15.0‡
γ_i	1.75	0.5
Z_{eff}	1.2	1.9
t_{ign} (sec)	3.0	3.0
β_p	0.21	0.20
W_{int} (MJ)	19.5	18.0
T_{eo} (keV)	16.7	15.5
τ_E (msec)	390	485
P_{OH} (MW)	7.1	8.1
P_α (MW)	50.0	37.0
P_B (MW)	7.1	8.6
P_{IC} (MW)	1.0	2.4
$Vol_{q=1}$ (%)	1.5	1.5

‡ $P_{INJ} \simeq 5$ MW for $1.2 < t < 1.8$ sec, 10 MW for $1.8 < t < 2.4$ sec, and 15 MW for $t > 2.4$ sec

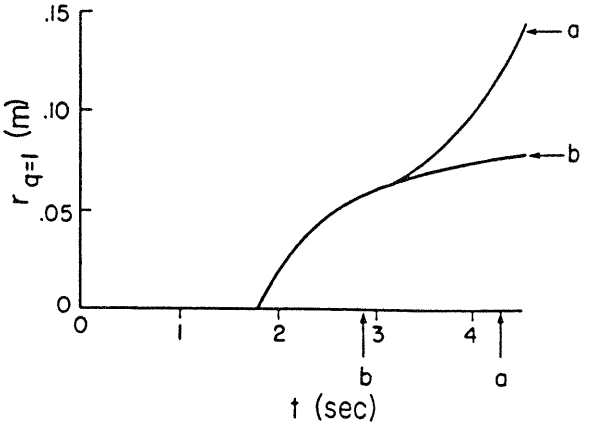

Fig. 11. Time evolution of the radius where $q = 1$ (on the horizontal midplane) for two cases of Table IX. (*a*) Reference case, (*b*) same case with 5 MW injected heating as in Fig. 10. Ignition, marked by arrows, is reached at 4.3 sec (*a*) and 2.9 sec (*b*). The appearance of a limiting time, when the $q = 1$ radius increases rapidly in the presence of ohmic heating alone, is delayed at the end of the flat top by injected heating

degraded discharge of Table III with $Z_{eff} = 1.6$. It must be noted that just 5 MW of injected heating are sufficient to achieve ignition immediately before (reference case, Table X and Fig. 10) or immediately after ($Z_{eff} = 1.6$, Table XI) the end of the current ramp. Table XII also illustrates two cases, at the maximum level of injected heating considered ($P_{INJ} \simeq 15$ MW for $t > 2.4$ sec), that marginally reach ignition. One has a large ion transport ($\gamma_i = 1.75$), while the other has a relatively high impurity level, $Z_{eff} = 1.9$. Both cases ignite shortly after the ramp, at $t \simeq 3$ sec with low energy confinement times ($\tau_E \simeq 390 \div 480$ msec) and a small volume where $q < 1$. Due to the higher peak temperatures ($16 \div 17$ keV) at ignition, the alpha heating power reaches relatively high levels ($P_\alpha \simeq 40 \div 59$ MW) and the thermal wall loading may limit the duration of the discharge.

In all the plasmas with injected heating, the $q \leqslant 1$ region remains very small until ignition (Fig. 11). It contains only the dip in q (that we do not consider realistic) caused by the specific form of the electrical resistivity adopted to take into account the effects of trapped electrons near the magnetic axis. These results were obtained using the same spatial ICRF heat deposition profile as suggested in Ref. [19]. This

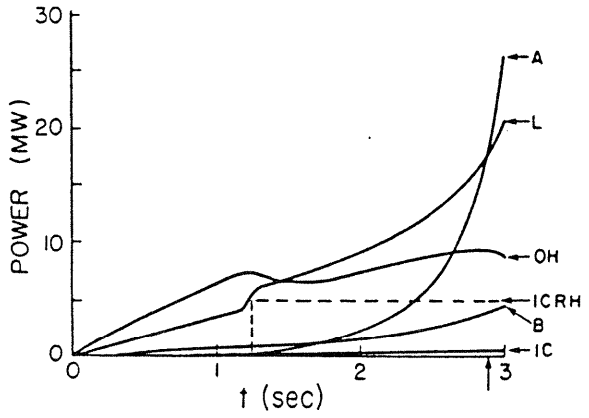

Fig. 10. Evolution of the volume integrated powers for an Ignitor plasma with 5 MW of injected ICRH heating (shown by dashed line). Initial parameters and current ramp are the same as for the reference case of Table II. Ignition is reached at 2.9 sec (arrow), with the volume of the $q \leqslant 1$ region very small

is of the form

$$S_{ICRH}(\Psi) \propto \frac{\left[1 - \left(\frac{\Psi - \Psi_{min}}{\Psi_{lim} - \Psi_{min}}\right)^2\right]}{\left[1 + \left(\frac{\Psi - \Psi_{min}}{\Psi_{lim} - \Psi_{min}}\right)^2 \frac{1}{(0.8)^2}\right]}$$

where Ψ is the poloidal magnetic flux, $\Psi = \Psi_{min}$ corresponds to the magnetic axis, and $\Psi = \Psi_{lim}$ corresponds to the edge of the plasma column. The effects of the fast ions induced by the ICRF waves were not considered.

Although we consider that sawtooth oscillations are unlikely to be excited in Ignitor due to the adopted four levels of protection against excitation of $m^o = 1$ modes (see Section 5.1), their time-averaged effect has been studied in a few cases, using the TSC sawtooth model. This model flattens the current density profile in the region where $q \leqslant 1$ by enhancing the neoclassical electrical resistivity and reduces the temperatures by enhancing the electron and ion thermal diffusivities by a factor 2 in this region. This model has been applied to reproduce the effects of sawteeth in the TFTR experiments carried out so far. Two cases are considered. The first one is the reference discharge, where the volume $Vol_{q=1}$ inside the surface where $q = 1$ is always small ($Vol_{q=1} < 6\%$ of the total plasma volume at ignition, Table I). As espected, no appreciable difference is found with the sawtooth model. The second case considers a degraded confinement ($\gamma_i = 1.0$ shown in Table III, case 2). Without the sawtooth model, the volume $Vol_{q=1}$ is about 24% of the total at ignition, but the temperature $T_{q=1}$ at the $q = 1$ surface when its volume becomes larger than 10% of the total is high ($\simeq 8.4$ keV), introducing a stabilizing feature against the onset of $m^o = 1$ modes. Table XIII shows that, if the sawtooth model is turned on, the plasma falls short of ignition ($P_\alpha/P_L \simeq 0.85$ at $t \simeq 4.7$ sec, $T_{eo} \simeq 10.6$ keV, with $\tau_E \simeq 605$ msec), without additional heating.

Finally we note that, except for a few degraded cases, all the simulations have values of $T_{q=1}$ larger than the value that we expect to be sufficient to produce effective stabilization or weakening of the $m^o = 1$ resistive modes (see Section 5.1) that can be excited within the $q = 1$ surface.

Table XIII. *Effect of the TSC sawtooth model for a degraded case*

	Degraded discharge	Sawtooth model
γ_i	1.0	1.0
t_{ign} (sec)	4.6	4.7*
β_p	0.14	0.14
W_{int} (MJ)	13.0	12.9
T_{eo} (keV)	12.9	10.6
τ_E (msec)	540	605
P_{OH} (MW)	8.4	10.3
P_α (MW)	24.0	18.2
P_B (MW)	4.2	5.3
P_{IC} (MW)	0.5	0.6

* Sub-ignited plasma with $P_\alpha/P_L \simeq 0.85$ and $\dot{W} \simeq 7.1$ MW

4.2. *Evolution of the current density profile*

The relatively slow inward diffusion of the plasma current, on the resistive time scale, also allows some control over the size of the region where the magnetic field line parameter $q \leqslant 1$. The numerical simulations show that during the current ramp the $q \leqslant 1$ region can be kept small or even nonexistent, depending upon the details of the current density distribution near the magnetic axis. The central temperature typically reaches levels of $4 \div 5$ keV by the end of the ramp. After the ramp, the $q \leqslant 1$ region continues to grow, but up to ignition its volume can be kept below 1/10 of the total. At the same time, when T_{eo} exceeds $5 \div 6$ keV, kinetic effects are found to stabilize (see Section 5.1) the resistive modes with poloidal mode number $m^0 = 1$ that are associated with sawtooth crashes, since the value of β-poloidal is quite small ($\beta_p \sim 0.1$). This temperature range also marks the onset of central fusion heating and at higher temperatures the high energy particle population, composed of the slowing down fusion alpha particles, is expected to provide an additional stabilizing influence [37]. This scenario is discussed in more detail in Section 5.1.

We have considered, as a practical criterion, that the excitation of $m^0 = 1$ modes should have little effect on ignition as long as the volume of the surface where $q = 1$ is less than 1/10 of the total plasma volume. For the Ignitor configuration this corresponds to $r/a \leqslant 1/3$. Recently, J. Manickam [38] has suggested a more generous criterion, on the basis of his analyses, corresponding to a horizontal radius about $0.4a$. These analyses refer to experiments carried out by the PBX-M machine where no losses of superthermal particles associated with the so-called "fishbone" oscillations are observed as long as this criterion is satisfied.

The simulation shows that this criterion can be satisfied until ignition for the energy confinement times discussed above, without external controls except programming of the current, magnetic field and plasma density rise. It is easy to keep the $q \leqslant 1$ region within half the minor radius at all times by lowering the plasma current after the initial ramp-up. Decreasing the current in this way does not have a significant adverse effect on attaining ignition, except in the marginal case. It also has little effect on the value of q near the magnetic axis, which continues to drop as the current is lowered, since the central current density diffuses inward as long as T_{eo} continues to rise rapidly. The size of the $q \leqslant 1$ region also depends on the details of the plasma temperature profile, and thus on the thermal transport. If the energy confinement does not degrade severely near ignition, ignition can be reached rapidly after the end of the current ramp and the $q \leqslant 1$ region remains small until past ignition, when the presence of fast α-particles can be effective additional stabilizing factor for the relevant $m^0 = 1$ modes [37]. On the other hand, larger transport losses or any other effects that lead to lower plasma temperatures in the outer half of the plasma column, during or after the ramp, increase the rate of penetration of the plasma current and thus increase the size of the $q \leqslant 1$ region at a given time.

The injection of electromagnetic waves at ion cyclotron frequencies can provide a further means of suppressing sawtooth oscillations before ignition, as demonstrated by results obtained by JET [39] and other machines. The Ignitor design makes provisions for up to 16 MW of injected power at frequencies $\simeq 130$ MHz. Our analysis shows that if injected heating at the level of $5 \div 15$ MW is applied, then the attainment of ignition can be accelerated significantly and the size of the $q \leqslant 1$ region kept small or nonexistent until well beyond ignition (Table IX–XII). Also, even if sawteeth are not completely suppressed, it can be shown that they do not prevent ignition if their period increases sufficiently with increasing temperature [40] or if their amplitude remains limited, as expected from the general behavior of the relevant $m^0 = 1$ resistive instabilities.

We note that it is not strictly necessary to keep the value of $q_\psi > 3$, at the edge of the plasma column, in order to ensure the plasma macroscopic stability, as shown by results obtained by the JET machine [41]. Nevertheless the machine design makes it possible to maintain $q_\psi \geqslant 3$ at all times by properly programming the current in the poloidal field coils [8]. In order to avoid internal reconnection activity, provisions are made to avoid the development of hollow or nonmonotonic toroidal current densities J_ϕ in the interior of the plasma. The free boundary simulation has shown [8] that the development of nonmonotonic J_ϕ profiles is related to the empirically derived JET stability boundaries in (l_i, q_ψ) space (normalized internal inductance l_i and edge magnetic safety factor q_ψ), when a collisional electrical resistivity that includes the effects of trapped electrons is assumed. The typical values of $l_i/2$ in Ignitor are reported in Table II for the reference discharge. In all the other simulations the values of $l_i/2$ were controlled to be similar by programming the current, density and magnetic field rise and plasma shape in a similar manner. Development of nonmonotonic profiles after the current ramp, which corresponds to slower inward current diffusion during the current ramp, is usually related to higher central q or smaller $q \leqslant 1$ regions. We may consider avoiding nonmonotonic profiles to be of less importance to the overall plasma stability than controlling the size of the $q \leqslant 1$ region, since the associated instabilities tend to be relatively mild in the regimes of interest.

The approach to D–T ignition by compact, high field experiments has also been investigated by a number of other authors [22, 42–44]. Almost all these studies started from a full size plasma with a fully penetrated current profile. A variety of thermal transport and sawtooth models have been used to show the importance of the plasma profiles and sawtooth effects on ignition. Other studies have shown that ignition remains possible if the sawtooth period increases sufficiently with temperature [40], as expected from theo-

retical considerations of plasma instabilities. Studies of the current ramp (for the BPX–CIT concept with strong injected heating [45] and in preliminary studies of the Ignitor [46]) also confirm that it is relatively easy to keep q_o above unity during the ramp.

In this context we point out that so far we have been the only group to simulate in detail [7, 8, 46] the process by which the plasma current is grown as the plasma radius is increased. Earlier analyses were unable to indicate a procedure by which the volume of the $q = 1$ region could be kept relatively small as the current is increased nor to assess properly the ohmic heating power up to ignition conditions. A further step that is needed is to refine the model for the current density transport, possibly along the lines suggested in Ref. [7].

5. Internal macroscopic modes

5.1. *Sawtooth oscillations* [7]

"Sawtooth" oscillations of the central part of the plasma column, associated with the instability of global plasma modes with dominant poloidal mode number $m^o = 1$, can prevent [4] the attainment of ignition, if their period is considerably shorter than the energy confinement time and the affected volume exceeds about 1/10 of the total, a prescription [47] that remains valid at present.

The ideal MHD stability parameter λ_H is of particular importance to assess the properties of these modes. The growth rate is defined as $\gamma_{MHD} = \lambda_H v_A/(R_o\sqrt{3})$, where v_A is the Alfvén velocity on the surface where $q = 1$, $\lambda_H \sim (r_1/R_o)^2(\beta_{p^*}^2 - \beta_{p^*}^{crit\,2})$, $\beta_{p^*} = 8\pi[\langle p\rangle_1 - p_1]/B_{p_1}^2$, where r_1 is the mean radius of this surface, p_1 and B_{p_1} the pressure and the poloidal magnetic field on it, and $\langle p\rangle_1$ the volume average pressure within the same surface [47]. The threshold $\beta_{p^*}^{crit}$, for which λ_H exceeds zero, deteriorates with increasing vertical elongation of the plasma cross section and improves with its triangularity. However, the triangularity that can realistically be produced is rather limited. Therefore the values of $\beta_{p^*}^{crit}$, and consequently of β_p^{crit}, for which $\lambda_H < 0$ can be relatively low [3]. In particular, a tight aspect ratio (that is, favorable) configuration such as that of Ignitor, where $R/a \simeq 2.7$ and the elongation is relatively modest, $\kappa \simeq 1.8$, has $\beta_p^{crit} \simeq 0.3 \div 0.35$ for $q_\psi \simeq 3 \div 3.5$ and realistic profiles of the plasma pressure and of the q parameter.

A high energy particle population, created by an injected heating system such as ICRH or by the α-particles produced by D–T reactions, can suppress the onset of sawtooth oscillations [38]. Therefore, to eliminate ideal MHD modes, it is advisable that β_p remain well below the value of β_p^{crit} that is obtained in the absence of a high energy particle population, until substantial D–T burning is produced and a considerable α-particle population is present. This is the strategy of Ignitor, that is designed to attain values of $\bar{B}_p = I_p(\mathrm{MA})/5\sqrt{ab}$, the average poloidal field, close to 4 T while programming the J_ϕ profile to maintain the volume where $q \leqslant 1$ relatively small. If a low $\bar{B}_p$ strategy is to be pursued instead, as in the case of the ITER studies [49], the total plasma current should be kept sufficiently low to maintain $q \geqslant 1$. This conflicts with the need to achieve the highest possible current in order to ensure maximum energy confinement under nonohmic conditions, at the high values of β_p that are then reached at ignition [3].

While the ideal MHD modes may be avoided, there remain resistive modes that are also macroscopic in nature, but become more benign as the plasma temperature increases [50]. In particular, there exists a relatively large region in parameter space where these modes are stable. This corresponds to temperatures where

$$\hat{\omega}_* = \omega_{*e}\tau_H/\varepsilon_\eta^{1/3} > 1,$$

where $\varepsilon_\eta \equiv \hat{s}^2 D_m/(r_1^2/\tau_H)$, $\tau_H \equiv \sqrt{3}\,R/v_A$, $\hat{s} \equiv \mathrm{d}\ln q/\mathrm{d}\ln r$, $D_m \equiv \eta_\parallel c^2/4\pi$, $\omega_{*e} \equiv -(1/r_1)(\mathrm{d}\ln n/\mathrm{d}r)(cT_e/eB)$, and n is the particle density. When $\lambda_H < 0$, the modes that can be excited are the so-called "strong resistive mode" modified by diamagnetic effects and the slower growing drift-tearing mode [50]. The former is an almost purely growing mode that occurs close to ideal MHD marginal stability, corresponding to large values of the jump $\Delta' \propto 1/|\lambda_H|$ in the derivative of the perturbed transverse magnetic field. The drift-tearing mode [50] is a propagating mode with frequency $\omega \simeq \omega_{*e}$ and occurs for smaller values of Δ', i.e., further away from ideal marginal stability [51]. Within the two fluid model, both modes are found to be stable [52, 53] in a wide "window" [53] of (positive) values of Δ', $1/(\omega_{*e}\tau_H) \sim \Delta_1' < \Delta' < \Delta_2' \sim (\omega_{*e}\tau_H/\varepsilon_\eta)^{1/2}$, when the effects of ion–ion collisions, that are stabilizing, are neglected. In this case, the growth rate in the drift tearing domain ($\Delta' < \Delta_1'$) is a nonmonotonic function of Δ' and is considerably smaller than that in the strong resistive mode domain ($\Delta' > \Delta_2'$). In reality, since the width of the layer where magnetic connection is induced by these modes becomes related to the ion gyroradius, the combined effects of ion–ion collisions and of finite Larmor radius are important [54]. A particle and momentum conserving operator, such as that used in [54], has been employed to derive the mode equation in the reconnection layer and solve it numerically over a wide range of temperatures [55]. Thus, for $\lambda_H \lesssim 0$, complete stability can be attained. For parameters typical of the Ignitor experiment, the strong resistive mode is found to be stable when the central temperature exceeds about 5 keV. Therefore the strategy that can be followed is that of programming the current density profile so that the volume of the region where $q = 1$ does not exceed about 1/10 of the total plasma volume (at $\kappa \simeq 1.8$) in order to limit the effects of the expected sawtooth oscillations, until this temperature is reached. From this point on, a moderate expansion of the $q = 1$ surface can be tolerated while regimes where a substantial population of α-particles, that add a further factor of stabilization, are achieved. In addition, r.f. waves at the ion cyclotron frequency, that create an anisotropic high energy population, can be injected in order to increase the stability margin against all resistive modes [37].

Recently, the rather large growth rates γ predicted long ago for collisionless modes [56], associated with the effects of finite electron inertia, have been confirmed [57] in the limit where the parameter $|\lambda_H| \lesssim \rho_i/r_1$, ρ_i being the ion gyro-radius. The excitation of these modes has been proposed as a possible explanation for the "crash" of the high temperature regimes that are experimentally obtained when the sawtooth oscillations attributed to resistive modes are suppressed. If this explanation proves to be reliable, the need to keep the parameter λ_H as negative as possible and

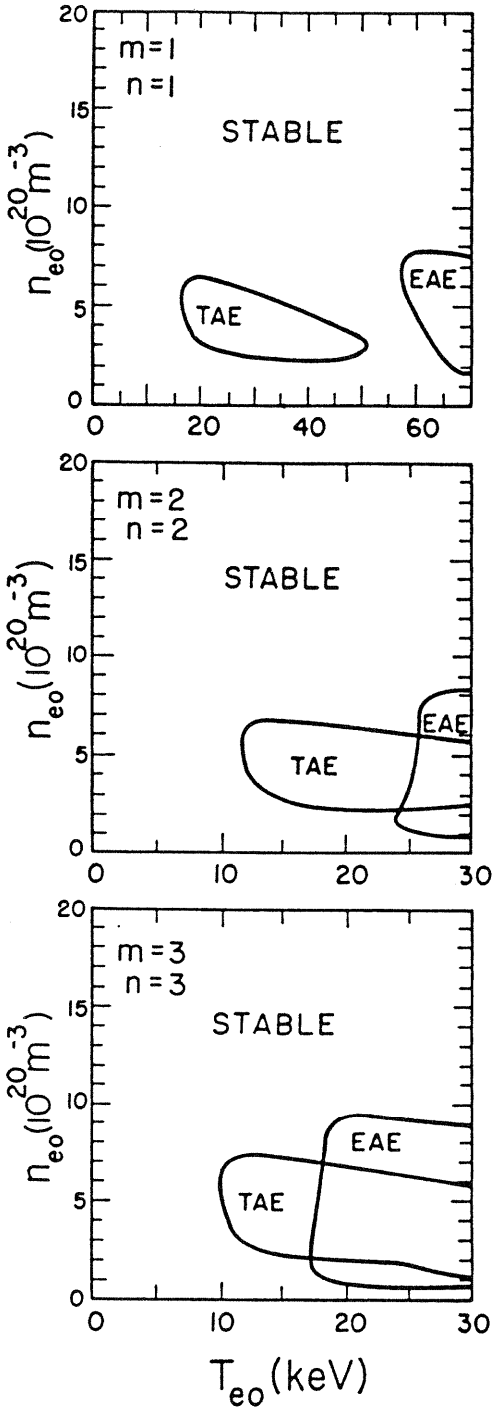

Fig. 12. Stability boundaries of low-n^o Alfvén gap modes (TAE and EAE) for Ignitor-like parameters. The Ignitor ignition regime ($n_{eo} \geq 10^{21}\,m^{-3}$ and $T_{eo} \leq 15\,keV$) lies in the stable regions

the volume of the $q \leq 1$ region relatively small becomes particularly compelling, for experiments that reach ignition with low degrees of plasma collisionality.

Finally, we note that recent experimental evidence supports the argument, made earlier on theoretical grounds, that producing peaked density profiles and thereby increasing the values of $\hat{\omega}_*$ and $\hat{\omega}_{*i} = \omega_{di}\tau_H/\varepsilon_\eta^{1/3}$ should enhance the stability against $m^o = 1$ modes. Here $\omega_{di} = (1/r_1)(dp_i/dr)c/(eBn)$. We refer for this to the experiments reported for instance in [58] and, in particular, to the fact that the possibility to suppress sawtooth oscillations by creating relatively peaked density profiles, in regimes where only ohmic heating is present, has been indicated as an explanation of the sawtooth free plasmas obtained by the ASDEX machines [59]. We notice that an objection had been raised to our repeated prediction, based on the stabilizing effect that the "diamagnetic" frequencies (ω_*), that depend on the plasma pressure gradients, have on $m^o = 1$ modes. The objection was that the development of a magnetic island tends to depress the electron temperature gradient over its extent because of the high thermal conductivity along the magnetic field lines. On the other hand, no similar argument could be raised against the density gradient. This is the origin of our expectation for the relevant stabilizing effect.

5.2. *Alfvén "gap modes"*

The Alfvén gap modes are macroscopic perturbations whose frequency lies in gaps in the Alfvén continuum spectrum arising because of toroidal (TAE) and elliptical (EAE) coupling [60, 61]. These global-type Alfvén waves can interact resonantly with circulating α-particles and be destabilized. Numerical simulations [62] have shown that a considerable fraction of α-particles can be lost due to α-particle orbit stochasticity induced by low-n^o Alfvén modes. Analytic expressions for the growth rates [63, 64], based on slowing down distribution functions of the α-particle population, show that the term driving the instability is proportional to $1/B$. Thus, high magnetic fields seem to raise the instability threshold. Figure 12, taken from Ref. [63], shows the stability boundaries of the TAE and EAE for Ignitor-like parameters. The expected Ignitor plasmas ($n_{eo} \gtrsim 10^{21}\,m^{-3}$ and $T_{eo} \lesssim 15\,keV$) are then predicted to be stable against low-n^o gap modes. As far as the high-n^o modes are concerned, both theory and recent neutral beam injection experiments [65], carried out by the DIII–D machine, have shown that modes of this type with $n^o \sim 5 \div 7$ can be the most unstable. However, the instability threshold observed in the experiments is substantially higher than the one predicted by the existing theory, which is not fully developed yet.

6. Conclusions

Compact high field experiments are shown to be suitable to produce low temperature ignition ($T_o \gtrsim 11\,keV$) of deuterium–tritium plasma mixtures with peak densities $n_o \simeq 10^{21}\,m^{-3}$, under known criteria of both energetics and stability. The plasma current that, in the considered cases, is raised to 12 MA, is gradually induced in the plasma column while its cross-section is increased. This process has been followed numerically for the free boundary plasma, using the TSC code. We have shown that the toroidal current density distribution can be controlled in such a way that the region where the magnetic winding parameter $\iota > 1$ ($q < 1$) has a relatively small volume. This is in fact one of the provisions that are made in order to avoid the onset of internal oscillations (so-called sawteeth) with relatively large amplitudes and frequencies that can prevent attaining ignition. At the same time the ohmic heating is maintained at relatively high levels up to ignition conditions, as the loop voltage retains a significant variation over the plasma radius.

As a consequence, when ignition is reached, the rate of α-particle heating does not exceed twice the rate of ohmic

heating. Under these conditions, the energy confinement time can be expected to be nearly immune to the deterioration that is observed in present day experiments with injected heating, when the ohmic heating becomes negligible relative to the externally applied heating. A degree of plasma purity, corresponding to $Z_{eff} \lesssim 1.6$, is required in order to attain ignition. This is expected to be ensured, on the basis of an extensive series of existing experimental observations, by the relatively high values of the plasma density that can be sustained. Our analysis confirms the fact that, since ignition can be attained by ohmic heating alone, injected heating systems in compact high field experiments should have the role of backups and be available, if needed, to suppress the possible onset of internal modes, within the surface where $\iota = 1$, to control the temperature and the current density profiles, and to accelerate the attainment of ignition.

The density profiles are assumed to be controllable by the known techniques of gas and pellet injection. The required minimum degree of peaking of these profiles, in order to achieve ignition under reasonable assumptions on the thermal transport and the formation of well-behaved current density distributions, is shown to be as low as $n_o/\langle n\rangle \simeq 1.5$ (see Fig. 8). The relevant values of β-poloidal are low, $\beta_p \lesssim 0.15$, so that a considerable safety margin against the onset of ideal MHD modes with poloidal number $m^o = 1$, within the surfaces where $\iota = 1$, can be maintained.

Acknowledgements

It is a pleasure to thank R. Englade for having been the first to demonstrate numerically the possibility to control the current rise, R. Betti for his contribution on the Alfvén gap modes, A. Airoldi and F. Pegoraro for their critical comments and contributions and S. C. Jardin and N. Pomphrey for their continuous support and unstinting effort on the TSC code.

This work was sponsored in part by the US Department of Energy and in part by the E.N.E.A. of Italy, under Contract N.90/38/3BLAO/88.

Appendix A. The ohmic thermal transport coefficient

A general electron anomalous thermal diffusion coefficient χ_e^{an} can be written [5] for steady state, ohmic plasmas that have a canonical temperature profile shape. In a general axisymmetric configuration, the thermal energy and particle balance equations for each species j can be written

$$\frac{\partial}{\partial t}\left(\frac{3}{2}p_j\right) + \frac{1}{V'}\frac{\partial}{\partial \xi}\left[V'\left(\langle\langle \mathbf{q}_j \cdot \nabla\xi\rangle\rangle + \left\langle\left\langle \frac{5}{2}p_j \mathbf{u}_j \cdot \nabla\xi\right\rangle\right\rangle\right)\right] - \langle\langle \mathbf{u}_j \cdot \nabla p_j\rangle\rangle = \langle\langle S_j^{th}\rangle\rangle + \langle\langle Q_j\rangle\rangle + \left\langle\left\langle \vec{\Pi} : \nabla \mathbf{u}_j\right\rangle\right\rangle. \quad (A.1)$$

$$\frac{\partial n_j}{\partial t} + \frac{1}{V'}\frac{\partial}{\partial \xi}\left[V'\langle\langle \Gamma_j \cdot \nabla\xi\rangle\rangle\right] = \langle\langle S_j\rangle\rangle \quad (A.2)$$

where ξ is a dimensionless toroidal flux surface variable $\xi = \xi(\Phi)$, $\langle\langle\cdots\rangle\rangle$ indicates the flux surface average, v is the volume enclosed by each surface, and

$$V'(\xi) \equiv \frac{\partial}{\partial \xi} V(\xi, t). \quad (A.3)$$

We choose the set of coordinates

$$(\xi, \theta, \phi)$$

where ϕ and θ are toroidal and poloidal coordinates respectively. Then we have

$$V'(\xi) = 2\pi \int_0^{2\pi} \sqrt{g}\, d\theta,$$

where $\sqrt{g}$ is the Jacobian,

$$\sqrt{g} \equiv |\nabla\xi \times \nabla\theta \cdot \nabla\phi|^{-1}, \quad (A.4)$$

and the flux surface average of a function A is defined by

$$\langle\langle A\rangle\rangle \equiv \int_0^{2\pi} \sqrt{g}\, A\, d\theta \Big/ \int_0^{2\pi} \sqrt{g}\, d\theta. \quad (A.5)$$

On the basis of these equations we may refer to several widely used plasma parameters:

(*i*) the toroidal loop voltage, a flux surface quantity,

$$V_\phi = 2\pi \frac{\langle\langle \mathbf{E} \cdot \mathbf{B}\rangle\rangle}{\langle\langle \mathbf{B} \cdot \nabla\phi\rangle\rangle} = 2\pi R E_\phi, \quad (A.6)$$

satisfying

$$\frac{\partial \iota(\xi, t)}{\partial t} = c\frac{\partial}{\partial \Phi} V_\phi, \quad (A.7)$$

where $\iota = q^{-1}$ is the magnetic twist parameter and Φ the toroidal magnetic flux within the surface ξ. Thus, under steady state conditions $V_\phi = V_\phi(\xi) = \text{const.}$

(*ii*) the ohmic heating source

$$\langle\langle S_{OH}\rangle\rangle = \langle\langle \mathbf{E} \cdot \mathbf{J}\rangle\rangle = \langle\langle E_\phi J_\phi\rangle\rangle \quad (A.8)$$

in steady state, when no current normal to the flux surface is driven, for example by an anisotropic pressure. In regimes with low β-poloidal and a tight aspect ratio, a significant poloidal current can be present in addition to J_ϕ.

(*iii*) the poloidal beta, that can be written as

$$\beta_p = \frac{20}{I_p^2}\int d\xi' p(\xi') \int_0^{2\pi} \sqrt{g}\,|\nabla\phi|\, d\theta \quad (A.9)$$

when the plasma pressure is measured in MPa and the total toroidal plasma current is I_p in MA. Here ξ_a indicates the outermost magnetic surface of the plasma.

(*iv*) the particle flux Γ_j, where the anomalous component for the electrons [32] can be written

$$\langle\langle \Gamma_e^{an} \cdot \nabla\xi\rangle\rangle = -D_p\left(\frac{\partial n_e}{\partial \xi} + 2\alpha_p^* n_e \frac{\rho}{\bar{a}^2}\frac{\partial \rho}{\partial \xi}\right)\langle\langle |\nabla\xi|^2\rangle\rangle, \quad (A.10)$$

where D_p and α_p^* are flux surface coefficients that depend on the plasma parameters and $\rho(\xi)$ is an arbitrary radial variable, such that $\rho \to \bar{a}$ on ξ_a, that should be chosen to represent the canonical profile chosen for the electron temperature, $T_e = T_{eo} \exp(-\alpha_T \rho^2/\bar{a}^2)$, as discussed below.

The "profile-consistent" form of the electron thermal diffusion coefficient $\chi_e(\xi, t)$ in axisymmetric geometry can be derived similarly to the cylindrical case. The electron energy balance, neglecting convection, satisfies the steady state relation

$$-\frac{1}{V'}\frac{\partial}{\partial \xi} V'\langle\langle \mathbf{q}_e \cdot \nabla\xi\rangle\rangle = \langle\langle S_{OH}\rangle\rangle + \langle\langle S_e\rangle\rangle, \quad (A.11)$$

where $\langle\langle S_{OH}\rangle\rangle$ and $\langle\langle S_e\rangle\rangle$ represent the flux surface averaged ohmic heating and the additional nonohmic, nondiffusive heating sources and sinks, respectively. Assuming that $\chi_e = \chi_e(\xi, t)$ is a flux surface function, we can also write

$$\langle\langle \mathbf{q}_e \cdot \nabla\xi\rangle\rangle = n_e \chi_e \frac{\partial T_e}{\partial \xi} \langle\langle |\nabla\xi|^2\rangle\rangle. \tag{A.12}$$

Integrating over ξ from the magnetic axis to a given flux surface,

$$\chi_e = -\frac{[P_{OH}(\xi) + P_e(\xi)]}{n_e(\partial T_e/\partial\xi)V'\langle\langle |\nabla\xi|^2\rangle\rangle} \tag{A.13}$$

where

$$P_{OH}(\xi) = \int^{\xi} d\eta V'(\eta)\langle\langle S_{OH}\rangle\rangle$$

and

$$P_e(\xi) = \int^{\xi} d\eta V'(\eta)\langle\langle S_e\rangle\rangle$$

are the volume integrated powers. The gradient $dT_e/d\xi$ is evaluated by invoking profile consistency [20], i.e., a canonical functional form for the profile, $T_e(r) = T_{eo} \exp[-\alpha_T l(\rho^2/\bar{a}^2)]$, where $l(\xi) \simeq \xi$, $l(0) = 0$ and $l(1) = 1$, and α_T is a weak function of ξ, following Coppi–Mazzucato [66, 21]. Here $\rho^2/\bar{a}^2$ reduces to r^2/a^2 in the large aspect ratio, circular flux surface limit. Then

$$\chi_e(\xi, t) = \frac{P_{He}(\xi)}{n_e T_e(2\alpha_T \rho/\bar{a}^2)l'} \frac{1}{\rho' V'\langle\langle |\nabla\xi|^2\rangle\rangle} \tag{A.14}$$

where $P_{He} \equiv P_{OH} + P_e$.

In steady state, the ohmic heating can be written $\langle\langle S_{OH}\rangle\rangle = (V_\phi/2\pi)\langle\langle J_\phi/R\rangle\rangle$, so that $P_{OH} = V_\phi I_\phi(\xi)$, where V_ϕ is constant across the plasma and I_ϕ is the toroidal current within a given flux surface. Then the considered form of the diffusion coefficient becomes

$$\chi_e = \frac{1}{(2\alpha_T \rho/\bar{a}^2)} \frac{(V_\phi/l')I_\phi(\xi)}{n_e T_e} f_N(\xi) \frac{1}{\rho' V'\langle\langle |\nabla\xi|^2\rangle\rangle}, \tag{A.15}$$

where $f_N(\xi) \equiv P_{He}(\xi)/P_{OH}(\xi)$.

Comparison with the large aspect ratio, circular cross section coefficient shows that, for $f_N \approx 1$,

(1) it is the toroidal component of the voltage and the plasma current that is important, rather than the component parallel to **B**, and

(2) the general canonical T_e profile can be expressed in a variety of ways that reduce to the same "profile consistent" form on circular flux surfaces. The choice should conform to available experiments.

We choose to define $\rho^2/\bar{a}^2 = V/V_a$, in terms of the flux surface volume v normalized to the total plasma volume v_a. Then, writing $\rho' V'\langle\langle |\nabla V|^2\rangle\rangle = (d\rho/dV)\langle\langle |\nabla V|^2\rangle\rangle$ and using $(2\rho/\bar{a}^2)(d\rho/dV) = 1/V_a$, the thermal diffusion coefficient becomes

$$\chi_e = \frac{(V_\phi/l')}{\alpha_T} \frac{I_\phi}{n_e T_e} \frac{V_a}{\langle\langle |\nabla V|^2\rangle\rangle} \tag{A.16}$$

and the consistent form for the density pinch term in eq. (A.10) is

$$-D_p \alpha_p^* n_e \frac{2\rho}{\bar{a}^2} \frac{\partial\rho}{\partial\xi} \langle\langle |\nabla\xi|^2\rangle\rangle = -D_p \alpha_p^* n_e \frac{V'}{V_a} \langle\langle |\nabla\xi|^2\rangle\rangle. \tag{A.17}$$

The voltage V_ϕ can be scaled [66, 21] in terms of a dimensionless quantity C_s chosen to represent the effects of current driven modes,

$$V_\phi = \varepsilon_s \bar{V}\left(\frac{R}{4a_I}\right) \tag{A.18}$$

$$e\bar{V}/l' = T_e C_s^{2/5} \tag{A.19}$$

$$C_s = \frac{v_s}{v_{ithe}} \omega_{pi} \frac{\nu_{ee}}{v_{ithe}^2} \frac{c^2}{\omega_{pe}^2}, \tag{A.20}$$

such that the scaled voltage $\bar{V}$ is approximately independent of T_e and ε_s is a numerical constant close to unity that must be determined from experiment. Using the boundary conditions $l(0) = 0$ and $l(1) = 1$, we find

$$e\bar{V} = \frac{1}{\int_0^1 d\left(\frac{\rho}{a}\right)^2 (T_e C_s^{2/5})^{-1}}. \tag{A.21}$$

Then (in cgs units)

$$\chi_e^{an} = \varepsilon_s \frac{1}{\alpha_T} \frac{1}{4e} \left(\frac{1}{3\sqrt{2}} c^2 e^3 \frac{m_e^2}{m_p}\right)^{2/5} \frac{R}{\bar{a}} \frac{I_\phi}{n_e^{4/5} T_e} \times \left(\frac{Z_* \Lambda_e}{A_i}\right)^{2/5} \frac{V_a}{\langle\langle |\nabla V|^2\rangle\rangle} f_N. \tag{A.22}$$

Approximating $R/(\bar{a}\alpha_T)$ by

$$\frac{1}{4\pi^2} \frac{V_a \pi^{3/2}}{A_a^{3/2}}, \tag{A.23}$$

where A_a is the area of the vertical cross section of the plasma, gives the version of χ_e^{an} in MKS units that we have used

$$\chi_e^{an} = \varepsilon_s C_{2D} \left(\frac{\pi^{3/2} V_a^2}{A_a^{3/2}}\right) \frac{I_\phi}{n_e^{4/5} T_e} \left(\frac{Z_* \Lambda_e}{A_i}\right)^{2/5} \times \frac{1}{\langle\langle |\nabla V|^2\rangle\rangle} \quad (\mathrm{m}^2/\mathrm{sec}), \tag{A.24}$$

where $C_{2D} = 1.04 \times 10^{12}$ and the numerical coefficient $\varepsilon_s \simeq 0.75$ has been found to fit many ohmic experiments, as described below. Here I_p in kA is the total plasma current, T_e is in keV, the subscript i represents the main ion species, and $Z_* \equiv A_i \sum_j Z_j^2 n_j/(n_e A_j)$ summed over all ions j can be approximated by $(n_i/n_e)Z_i^2 + (1/2)A_i(1 - n_i Z_i/n_e)$, A_j is the atomic weight of ion j in amu, and Λ_e the Coulomb logarithm.

The radial variation of the diffusion coefficient differs somewhat from the cylindrical case. In particular, the geometric factor $\rho' V'\langle\langle |\nabla\xi|^2\rangle\rangle$ depends on the form chosen for the canonical T_e profile. The choice made here implies that configurations with significant vertical elongation should have broader temperature profiles, when viewed in the horizontal midplane, than circular plasmas with similar values of α_T.

The numerical constant ε_s that scales the voltage has been determined by comparison with experiment, using the cylindrical form of the diffusion coefficient. Numerical simulations of ohmic TFTR results [67] showed that $\varepsilon_s = 0.75 \pm 20\%$ reproduced the discharges within a 10% variation around the measured Z_{eff}, P_R, $T_e(r)$ in the central region,

and the surface voltage V_S, for the cases where the uncertainties of the power lost to the thermal transport were small enough to allow a meaningful comparison (in general, these were cases in which the impurity induced radiation power loss was small to moderate relative to the ohmic heating). In Alcator A and Frascati Torus (FT), where ohmic heating dominated the electron energy balance and sawtooth oscillations were small or nonexistent, it had the value 0.72–0.78 for deuterium plasmas, increasing with q_a [68]. Varying the magnitude by $\pm 25\%$ produced a $\pm 10\%$ change in T_{eo}. Values close to the given fit ohmic discharges in Alcator C, Pulsator, and FT [69], in a different transport code. Similar expressions for χ_e^{an} can describe ohmic discharges in TEXT, where $\varepsilon_s = 0.735 Z_{eff}^{0.4}$ for relatively clean plasmas [70], and JET, where the normalization depends upon assumptions made on the ion transport [71]. Pellet-injected and IOC (improved ohmic confinement) plasmas in ASDEX have also been found to be well described by the value used for TFTR.

References

1. Coppi, B., "High Current Density Tritium Burner" (R.L.E. Report PRR-75/18) (Massachusetts Institute of Technology, Cambridge 1975); Comm. Plasma Phys. Cont. Fusion **3**, 2 (1977).
2. Boxman, G. J., Coppi, B., De Koch, L. C., Meddens, B. J., Oomens, A. A., Ornstein, L. Th., Pappas, D. S., Parker, R. R., Pieroni, L., Segre, S. E., Schüller, F. C. and Taylor, R. J., "Proc. 7th Eur. Conf. on Plasma Physics, 1976" (Ecole Polytechnique Fédérale de Lausanne, Switzerland 1975), Vol. 2, p. 14.
3. Coppi, A. C. and Coppi, B., "Stability of Internal Global Modes in Advanced Plasma Confinement Configurations" (R.L.E. Report PTP-88/17) (Massachusetts Institue of Technology, Cambridge, MA 1989); in press for Nuclear Fusion.
4. Coppi, B., Taroni, A. and Cenacchi, G., in: "Plasma Physics and Controlled Nuclear Fusion Research 1976" (Proc. 6th Int. Conf., Berchtesgaden) (I.A.E.A., Vienna 1977), Vol. 1, p. 487.
5. Coppi, B. and Sugiyama, L., "A Thermal Transport Coefficient for Well-confined Plasmas" (R.L.E. Report PTP-89/18) (Massachusetts Institute of Technology, Cambridge, MA 1989).
6. Lackner, K. and Gottardi, N. A. O., Nucl. Fusion **30**, 767 (1990).
7. Coppi, B., Englade, R., Nassi, M., Pegoraro, F. and Sugiyama, L., in: "Plasma Physics and Controlled Nuclear Fusion Research 1990" (Proc. 13th Int. Conf., Washington) (I.A.E.A., Vienna 1991), paper CN-53/D-4-14.
8. Sugiyama, L. and Nassi, M., "Free Boundary Current Ramp and Current Profile in a D–T Ignition Experiment" (R.L.E. Report PTP-90/8) (Massachusetts Institute of Technology, Cambridge, MA 1990); submitted to Nuclear Fusion.
9. Suzuki, N., *et al.*, in: "Plasma Physics and Controlled Nuclear Fusion Research, 1988" (Proc. 12th Int. Conf., Nice) (I.A.E.A., Vienna 1989), Vol. 1, p. 207.
10. Coppi, B., Rosenbluth, M. N. and Sagdeev, R. Z., Phys. Fluids **10**, 582 (1967).
11. Coppi, B., Cowley, S., Detragiache, P., Kulsrud, R., Pegoraro, F. and Tang, W. M., in: "Plasma Physics and Controlled Nuclear Fusion Research, 1984" (Proc. 10th Int. Conf., London) (I.A.E.A., Vienna 1985), Vol. 2, p. 93; Coppi, B. and Tang, W. M., Phys. Fluids **31**, 2683 (1988).
12. Sigmar, D. J., *et al.*, in: "Plasma Physics and Controlled Nuclear Fusion Research, 1990" (Proc. 13th Int. Conf., Washington) (I.A.E.A., Vienna 1991), paper CN-53/G-1-1.
13. Coppi, B., Vuoto **18**, 153 (1988).
14. Coppi, B. and The Ignitor Group, in: "Plasma Physics and Controlled Nuclear Fusion Research, 1988" (Proc. 12th Int. Conf., Nice) (I.A.E.A., Vienna 1989), Vol. 3, p. 357.
15. Helton, F. J., "Dignitor PFC System Design" (Report GA-C 20161) (General Atomics, San Diego, CA 1990); Bromberg, L., Titus, P., Cohn, D. R. and Bolton, C. W., "Ignitor Scale-up Studies (DIGNITOR)" (Report PFC/RR-90-5) (Massachusetts Institute of Technology, Cambridge, MA 1990).
16. Nassi, M., "Volt-sec Requirement and Relevant Margin in the Ignitor Device" (R.L.E. Report PTP-90/1) (Massachusetts Institute of Technology, Cambridge, MA 1990).
17. Terry, J. L., *et al.*, in: "Plasma Physics and Controlled Nuclear Fusion Research, 1990" (Proc. 13th Int. Conf., Washington) (I.A.D.A., Vienna 1991), paper CN-53/A-5-5.
18. Coppi, B. and Sugiyama, L., Comm. Plasma Phys. Cont. Fus. **10**, 43 (1987).
19. Jardin, S. C., Pomphrey, N. and Delucia, J., J. Comp. Phys. **66**, 481 (1986).
20. Coppi, B., Comm. Plasma Phys. Cont. Fusion **5**, 261 (1980).
21. Coppi, B. and Mazzucato, E., Phys. Rev. Lett. **71A**, 337 (1979).
22. Englade, R. C., Nucl. Fusion **29**, 999 (1989).
23. Coppi, B. and Rewoldt, G., Phys. Rev. Letters **33**, 1329 (1974); Coppi, B. and Pegoraro, F., Nucl. Fusion **17**, 963 (1977).
24. Coppi, B., Furth, H. P., Rosenbluth, M. N. and Sagdeev, R. Z., Phys. Rev Lett. **17**, 377 (1966).
25. Coppi, B., in: "Plasma Physics and Controlled Nuclear Fusion Research, 1990" (Proc. 13th Int. Conf., Washington) (I.A.E.A., Vienna 1991), paper CN-53/I-2-6.
26. Coppi, B., Comm. Plasma Phys. Cont. Fusion **12**, 319 (1989).
27. Chang, C. S. and Hinton, F. L., Phys. Fluids **29**, 3314 (1986).
28. Schissel, D. P., DeBoo, J. C., Grüber, O., Kardaun, O., Ryter, F. and Wagner, F., "H-mode Energy Confinement Scaling from ASDEX, DIII-D, and JET Tokamaks" (Report GA-A20548) (General Atomics, San Diego, CA 1991); to be published in the Proceedings of the 18th EPS Conference on Controlled Fusion and Plasma Heating, June 3–7, Berlin (1991).
29. Simonen, T. C., Jackson, G. L., Hodapp, T., Holtrop, K., Phillips, J., Winter, J. and The DIII-D Team, "VH-mode: a New Very High Confinement Regime in the Boronized DIII-D Tokamak" (Report GA-A20552) (General Atomics, San Diego, CA 1991); to be published in the Proceedings of the 18th EPS Conference on Controlled Fusion and Plasma Heating, June 3–7, Berlin (1991).
30. Hirshman, S. P., Hawryluk, R. J. and Birge, B., Nucl. Fusion **17**, 611 (1977).
31. Singer, C. E., *et al.*, Computer Phys. Comm. **49**, 275 (1988).
32. Coppi, B. and Sharky, N., Nucl. Fusion **21**, 1363 (1981).
33. Kaye, S. M. and Goldston, R. J., Nucl. Fusion **25**, 65 (1985).
34. Rebut, P. H., Lallia, P. P. and Watkins, M. L., in: "Plasma Physics and Controlled Nuclear Fusion Research, 1988" (Proc. 12th Int. Conf., Nice) (I.A.E.A., Vienna 1989), Vol. 2, p. 191.
35. Kaye, S. M., *et al.*, Phys. Fluids **B2**, 2926 (1990).
36. Yushmanov, P. N., *et al.*, Nucl. Fusion **30**, 1999 (1990).
37. Coppi, B., Detragiache, P., Migliuolo, S., Pegoraro, F. and Porcelli, F., Phys. Rev. Lett. **63**, 2733 (1989).
38. Manickam, J., Roberts, D., Kaita, R., Leviton, F., Okabayashi, M. and White, R. B., "The Role of the Internal Kink Mode in Experiments" in: "Proceedings of the 1990 International Sherwood Theory Conference" (College of William and Mary, Williamsburg, VA 1990).
39. Campbell, D., *et al.*, in: "Plasma Physics and Controlled Nuclear Fusion Research, 1988" (Proc. 12th Int. Conf., Nice) (I.A.E.A., Vienna 1989), Vol. 1, p. 377.
40. Coppi, B. and Englade, R., "Sawtooth Oscillations and Ignition" (R.L.E. Report PTP-89/12) (Massachusetts Institute of Technology, Cambridge, MA 1989).
41. Lomas, P. J., Green, B. J., How, J. and The JET Team, Plasma Phys. Cont. Fusion **31**, 1481 (1989).
42. Airoldi, A. and Cenacchi, G., Fusion Technology **19**, 78 (1991).
43. Airoldi, A. and Cenacchi, G., Plasma Phys. Cont. Fusion **33**, 91 (1991).
44. Connor, J. W., "Anomalous Transport and Ignition" (AEA Fusion Report) (Culham Laboratory, Abingdon, UK 1990).
45. Houlberg, W. A., Nucl. Fusion **27**, 1009 (1987).
46. Nassi, M., *et al.*, Bull. Am. Phys. Soc. **35**, 2131 (1990).
47. Coppi, B., Crew, G. B. and Ramos, J. J., Comm. Plasma Phys. Cont. Fusion **6**, 109 (1981).
48. Bussac, M. N., Pellat, R., Edery, D. and Soulé, J. L., Phys. Rev. Lett. **35**, 1638 (1975).
49. Tomabechi, K., in: "Plasma Physics and Controlled Nuclear Fusion Research, 1990" (Proc. 13th Int. Conf., Washington) (I.A.E.A., Vienna 1991), paper CN-53/F-1-1.
50. Ara, G., *et al.*, Ann. Phys. **112**, 443 (1978).

51. Bussac, M. N., Edery, D., Pellat, R. and Soulé, J. L., in: "Plasma Physics and Controlled Nuclear Fusion, 1986" (Proc. 11th Int. Conf., Kyoto) (I.A.E.A., Vienna 1987), Vol. 1, p. 607.
52. Coppi, B., Englade, R., Migliuolo, S., Porcelli, F. and Sugiyama, L., in: "Plasma Physics and Controlled Fusion, 1986" (Proc. 11th Int. Conf., Kyoto) (I.A.E.A., Vienna 1987), Vol. 3, 397.
53. Porcelli, F., Migliuolo, S. and Pegoraro, F., Europhysics Conference Abstracts **14BII**, 898, (1990); Migliuolo, S., Pegoraro, F., and Porcelli, F., Phys. Fluids **B3**, 1338 (1991).
54. Coppi, B. and Rosenbluth, M. N., in: "Plasma Physics and Controlled Nuclear Fusion Research, 1965" (Proc. 1st Int. Conf.) (I.A.E.A., Vienna 1966), Vol. 1, p. 617.
55. Migliuolo, S., Nucl. Fusion **31**, 365 (1991).
56. Coppi, B., Phys. Letters **11**, 226 (1964).
57. Coppi, B. and Detragiache, P., "Magnetic Topology Transitions in Collisionless Plasmas" (R.L.E. Report PTP-90/14) (Massachusetts Institute of Technology, Cambridge, MA 1990); submitted to Phys. Rev. Letters.
58. Kaufman, M., *et al.*, in: "Plasma Physics and Controlled Nuclear Fusion Research, 1988" (Proc. 12th Int. Conf., Nice) (I.A.E.A., Vienna 1989), Vol. 1, p. 229.
59. Stroth, U., Fussmann, G., Kreiger, K., Mertens, V., Wagner, F., Bessenrodt-Weberpals, M., Büchse, R., Giannone, L., Herrmann, H., Simmet, E., Steuer, K. H. and The ASDEX Team, "Sawtooth-free Ohmic Discharges in ASDEX and the Aspects of Neoclassical Ion Transport" (Institut für Plasma-physik, Report IPP 111/178) (Garching bei München, Germany 1991); submitted to Nuclear Fusion.
60. Cheng, C. Z. and Chance, H. S., Phys. Fluids **29**, 3659 (1986).
61. Betti, R. and Freidberg, J. P., Phys. Fluids (in press, 1991).
62. Sigmar, D. J., Hsu, C. T., White, R. and Cheng, C. Z., "Alpha Particle Losses from Toroidicity Induced Alfvén Eigenmodes" (P.F.C. Report PFC/JA-89-58) (Massachusetts Institute of Technology, Cambridge, MA 1989); presented at the IAEA Technical Committee Meeting on "Alpha Particles Confinement and Heating", October 1989, Kiev, USSR.
63. Fu, G. Y. and Van Dam, J. W., Phys. Fluids **B1**, 1949 (1989).
64. Betti, R. and Friedberg, J. P., "Stability of Alfvén Gap Modes in Burning Plasmas" (P.F.C. Report PFC/JA-91-25) (Massachusetts Institute of Technology, Cambridge, MA 1991); submitted to Physics of Fluids.
65. Heidbrink, W. W., Strait, E. J., Doyle, E., Sager, G. and Snider, R., "An Investigation of Beam-driven Alfvén Instabilities in the DIII-D Tokamak" (Report GA-A20254) (General Atomics, San Diego, CA 1991); in print on Nuclear Fusion.
66. Coppi, B., Fiz. Plasmy **11**, 83 (1985).
67. Sugiyama, L. and Efthimion, P., "Predictive Transport Simulation of TFTR Ohmic Discharges" (R.L.E. Report PTP-89/14) (Massachusetts Institute of Technology, Cambridge, MA 1989).
68. Humphreys, D. and Sugiyama, L., Sherwood Theory Meeting, Arlington, VA (1983). paper 1S26.
69. Grüber, O., Nucl. Fusion **22**, 1349 (1982).
70. Miner, W. H., Ross, D. W., Ware, A. A. and Wiley, J. C., Sherwood Theory Meeting, San Diego, CA (1985), paper 2Q8.
71. Taroni, A. and Tibone, F., in: "Controlled Fusion and Plasma Physics" (Proc. 12th Europ. Conf., Schliersee, 1986), (European Physical Society, Garching 1987).